Two dynamically distinct circuits driving inhibition in sensory thalamus

Rosa I. Martinez-Garcia[1,2,5], Bettina Voelcker[1,3,5], Julia B. Zaltsman[1], Saundra L. Patrick[1], Tanya R. Stevens[1], Barry W. Connors[1], Scott J. Cruikshank[1,4*]

[1]Department of Neuroscience
[2]Department of Molecular Biology, Cell Biology, and Biochemistry
Division of Biology & Medicine
Brown University
Providence, RI 02912

[3]Present address of Bettina Voelcker:
Center for Neural Science
New York University
New York, NY 10003

[4]Present address of Scott Cruikshank:
Department of Neurobiology
University of Alabama at Birmingham
Birmingham, AL 35294

[5] These authors contributed equally to this work

*e-mail: sjc@uab.edu

Abstract

Most sensory information destined for the neocortex is relayed there from the thalamus, where considerable transformation occurs[1,2]. One powerful means of transformation involves interactions between excitatory thalamocortical neurons that carry data to cortex and inhibitory neurons of the thalamic reticular nucleus (TRN) that regulate flow of those data[3-6]. Despite enduring recognition of the TRN's importance[7-9], understanding of its cell types, their organization, and their functional properties has lagged that of the thalamocortical systems it controls.

Here we address this, investigating somatosensory and visual circuits of the TRN. First, in the somatosensory TRN we observed two groups of genetically defined neurons that are topographically segregated, physiologically distinct, and connect reciprocally with independent thalamocortical nuclei via dynamically divergent synapses. Calbindin-expressing cells, located in the central core, connect with the ventral posterior nucleus (VP), the primary somatosensory thalamocortical relay. In contrast, somatostatin-expressing cells, residing along the surrounding edges of TRN, synapse with the posterior medial thalamic nucleus (POM), a higher-order structure that carries both top-down and bottom-up information[10-12]. The two TRN cell groups process their inputs in pathway-specific ways. Synapses from VP to central TRN cells evoke rapid currents that depress deeply during repetitive activity, driving phasic spike output. In contrast, synapses from POM to edge TRN cells evoke slower, sustained currents that drive more persistent spiking. Differences in intrinsic physiology of TRN cell types, including state-dependent bursting, also contribute to these output dynamics. Thus, processing specializations of the two TRN circuits appear to be tuned to the types of signals they carry—the primary central circuit to discrete sensory events, and the higher-order edge circuit to temporally distributed signals integrated from multiple sources. Central and edge circuits of the visual TRN and their associated thalamocortical nuclei closely resemble those of the somatosensory circuits. These results provide fundamental insights about how subnetworks of TRN neurons could differentially process distinct classes of thalamic information.

Results

We first explored the cellular composition of the TRN, characterizing expression of parvalbumin (PV), calbindin (CB), and somatostatin (SOM)—three markers previously found to be useful in differentiating functionally distinct neural types in the neocortex and elsewhere[13]. Brain sections spanning the somatosensory sector of the TRN[4,7,8] were prepared from SOM-Cre mice that had been crossed with a Cre-dependent tdTomato (tdT) reporter, then stained immunohistochemically for CB and PV (Fig. 1a). All somatosensory sector TRN cells expressed PV[1,14], whereas only subsets exhibited SOM-tdT or CB labeling (~64% and ~48%, respectively; Fig. 1a, c; Extended Data Fig. 1-2).

SOM-tdT and CB cells had largely complementary distributions across the somatosensory sector of the TRN. SOM-tdT cells were at their highest densities near the medial and lateral edges of the sector, whereas CB cells were concentrated near the center and virtually absent along the edges (Fig. 1a, c; Extended Data Fig. 1, 3). Quantitative comparisons between the medial 20%, lateral 20% and central 60% of the somatosensory TRN confirmed that. The proportion of cells expressing SOM-tdT was significantly higher in the edge zones than in the central zone ($p < 0.0001$), while the reverse was true for CB ($p < 0.0001$) (Fig. 1c).

To test this possible complementary organization further, we used *in situ* hybridization to assay SOM, CB, and PV mRNA expression (Fig. 1b). The highest SOM cell densities were again found in the medial and lateral edge zones, CB cells were clustered in the central zone, and nearly all cells were PV positive (Fig. 1b, d; Extended Data Fig 4). Interestingly, the edge vs. central segregation of the SOM and CB cells was considerably more salient in the mRNA assay (cf. Fig. 1a to 1b), mainly due to decreased proportions of SOM cells in the central zone (only 15.3 ± 2.2% of central cells expressed SOM mRNA whereas 54.7% expressed SOM-Cre x tdT; Figs. 1c-d, right, Extended Data Fig. 4).

The near absence of SOM mRNA in the central zone suggests that most neurons located there may not actually express SOM protein in mature animals, and that the central cells with tdT in the crossed SOM-Cre x tdT reporter mice could result from genetic recombination early in development, with persistent tdT expression thereafter[15]. To test for mature SOM expression, we initially tried immunohistochemistry but were unable to find SOM antibodies adequate for TRN (data not shown). As an alternative, we assayed Cre expression in mature SOM-Cre mice, injecting an adeno-associated virus (AAV) driving Cre-dependent GFP (AAV2/9-DIO-GFP) in their TRNs. We found that Cre expression in the somatosensory TRN of these mice is almost entirely restricted to the edge zones, consistent with the SOM mRNA pattern (Fig. 1b, d, e, Extended Data

Figs. 5-6). Together, the results indicate that the somatosensory sector of TRN is composed of neurochemically distinct cell types segregated into separate zones: a core central zone is composed mostly of CB-expressing neurons, and it is flanked by edge zones composed of SOM-expressing neurons.

First-order VP and higher-order POM thalamocortical (TC) nuclei transmit distinct information to different targets in the neocortex and send collaterals to the TRN, the latter leading to both open- and closed-loop thalamic inhibition[4-6,8]. Clarifying the organization of these circuits, including how first-order and higher-order TC nuclei synapse with specific subsets of TRN neurons[16], is essential to understanding thalamic information processing[7]. To this end, we selectively expressed ChR2-eYFP in either VP or POM (via stereotaxic virus injections) and characterized their inputs to TRN (Fig. 2). Strikingly, the thalamocortical collateral projections to TRN segregated topographically in close alignment with the previously observed patterns of TRN cell subtypes. VP axons terminated in the CB-rich central zone of the somatosensory TRN, whereas POM axons terminated along the SOM-dense medial and lateral edges (Fig. 2a-b; Extended Data Fig. 7a, 8a).

Given this stark anatomical segregation of VP and POM projections, and the observation that TRN dendrites generally run parallel to the plane of the nucleus, it seemed likely that central and edge TRN cells would be selectively targeted by synapses from VP and POM, respectively. However, TRN cell dendrites might have spans sufficient to reach afferents terminating in adjacent zones, leading to functional cross-talk among these otherwise distinct circuits[1,8,17]. To address this, we mapped synaptic strengths of POM and VP inputs to TRN cells located across the mediolateral axis of the somatosensory TRN (Fig. 2c-j). Consistent with the anatomical projection patterns, responses evoked by activation of POM inputs were much stronger for medial and lateral edge cells than for central cells (Fig. 2c-e; Extended Data Fig. 7b), whereas VP inputs evoked their strongest responses in central cells (Fig. 2g-i; Extended Data Fig. 8b). Moreover, synaptic strengths for TRN cells correlated with fluorescence intensities of the afferent terminals near their soma (Fig. 2d, f, h, j). Together, our findings show that primary and higher-order somatosensory inputs to TRN are topographically segregated and align with the neurochemical pattern of TRN cell types: VP projects most strongly onto the CB-expressing central cells and POM projects most strongly onto SOM-expressing edge cells.

Primary and higher-order thalamocortical nuclei convey qualitatively different types of information[10,12,18-22], and we wondered if VP and POM communication with TRN might involve parallel differences in synaptic processing mechanisms. To address this, we compared the dynamic features of the glutamatergic synaptic currents (kinetics and short-term synaptic

depression) evoked by photostimulating VP and POM inputs to central and edge TRN cells, respectively. VP synaptic currents in central TRN cells were brief and depressed deeply during repetitive activation (Fig. 3a-c; Extended Data Fig. 9-12). Conversely, POM currents in TRN edge cells were longer-lasting and more stable during repetition (Fig. 3a-c, Extended Data Fig. 10-12).

To understand how these dynamically distinct synaptic inputs to TRN neurons might be integrated postsynaptically, we assessed the cells' intrinsic physiological characteristics. Central and edge TRN neurons differed across a range of passive and active membrane properties[17]. Edge cells had higher resistances, lower capacitances, and smaller somata than central cells (Extended Data Fig.13-14, Extended Data Table 1). Action potential kinetics, afterpotentials and threshold currents also differed (Extended Data Fig. 13; Extended Data Table 1). One striking intrinsic distinction among TRN cell types, which is likely to have powerful effects on responses to synaptic input during certain behavioral states[1,2,5,6,23-27], was the much greater tendency of central cells to fire action potentials in high frequency bursts (Fig 3d; Extended Data Table 1). The bursting differences were consistent with greater T-type (low threshold-activated) calcium currents in the central cells[17,28-31]. Thus, nearly all central cells fired bursts following release from hyperpolarizing stimuli (V_m set at -92 mV with intracellular current, followed by current termination), with an average of ~9 spikes each. In contrast, under matched stimulus conditions, most edge cells either failed to burst or fired weak bursts (average ~2 spikes; Fig 3d; Table 1). Neither cell type exhibited bursting when excited from a more depolarized steady-state V_m (~-74 mV; Extended Data Fig. 13).

We next examined how the distinctive pathway-specific properties of synaptic inputs and the cell type-specific intrinsic properties of edge and central cells combine to control the spiking responses of TRN cells to their excitatory thalamic inputs. The brief and depressing synaptic inputs from VP to central TRN cells, together with the propensity of central cells to burst, suggests they might respond to VP inputs with phasic spike patterns – initially high firing rates that quickly drop with repeated stimulation. In contrast, the kinetically slow and more stable inputs from POM to the less intrinsically bursty edge cells predict initially weaker but more sustained spiking.

First, we generated simulated synaptic currents that matched the waveforms previously recorded from central and edge TRN cells in response to their VP and POM inputs, respectively. We then characterized the postsynaptic TRN spike patterns elicited by intracellular injection of these synaptic currents, delivered while the TRN cells were at their resting potentials (~ -84 mV). As predicted, central cells responded to the simulated VP synaptic inputs with initial bursts that strongly depressed with repetitive activation. In contrast, the spiking responses of edge cells to

the simulated POM inputs were initially much weaker but were more persistent during repetitive activation (Fig. 4a-b).

Did differences in intrinsic bursting (Fig. 3d, Extended Data Table 1) contribute to these striking differences in synaptically evoked spike outputs? To address this, we depolarized the TRN cells to -74 mV to partially inactivate T-type calcium channels and reduce intrinsic bursting, then recharacterized the cells' responses to the simulated synaptic currents. Central TRN responses became far less phasic and fired more persistently when tonically depolarized, whereas edge cell responses were barely affected (Fig. 4c). Without intrinsic bursts, initial spiking was greatly reduced in central cells (41% reduction for stimulus 1) but only modestly reduced in edge cells (23%), and responses to later stimuli in the trains were enhanced more for central than edge cells (Fig. 4c). These results indicate that intrinsic bursting in central TRN cells has a powerful role in their responses to excitatory thalamic inputs when that input arrives during relatively hyperpolarized states (e.g., during sleep or periods of strong inhibition). In contrast, the far smaller effects of polarization on edge cell spiking indicates less influence of T-type calcium bursting and, importantly, weaker modulation by the kinds of membrane potential changes thought to occur during shifts in behavioral state[1,6,23-27,32].

Finally, we wondered whether the dynamic features of the faster, more depressing VP synaptic inputs to central cells (Fig. 3) also contributed to the more phasic nature of central cell spike outputs. For this we generated simulated synaptic currents that were the average, in terms of EPSC kinetics and short-term synaptic depression, of the natural VP → central and POM → edge synaptic currents, and tested their effects on evoked spiking. Cells were set to steady-state membrane potentials of -74 mV to minimize differences due to bursting (as in Fig 4c, above). Remarkably, the responses of the two cell types were virtually identical when triggered by the averaged synaptic input; the central cell responses became more sustained and the edge responses slightly more phasic (Fig. 4c vs 4d). Thus, the different properties of the synaptic inputs clearly contribute to the specific response patterns of the two TRN cell types. Together, these results indicate that central and edge cells differentially transform their native excitatory thalamic inputs into distinct spiking outputs through differences in both the dynamics of their synaptic inputs and their intrinsic burstiness.

To better understand the consequences of the output from the distinct TRN subcircuits, we examined their projections and the inhibitory feedback they produce. Interestingly, the two TRN cell types selectively inhibit the thalamocortical nuclei that drive them. That is, CB-expressing central TRN cells project to and inhibit VPM neurons, whereas SOM-expressing edge cells

bypass the VPM and instead inhibit POM (Extended Data Fig. 15). Thus, the primary and higher order segregation of somatosensory reticulothalamic subcircuits appears to be largely reciprocal.[8,16,33]

To test whether other sensory thalamic systems might share the salient structural-functional organization described here, we studied the visual TRN and its associated thalamocortical nuclei—the primary dorsal lateral geniculate and the higher-order lateral posterior nucleus (sometimes called the pulvinar). Remarkably, the organization of the visual TRN, in terms of both synaptic input patterns from primary and higher-order thalamocortical nuclei and intrinsic physiological properties of the TRN neurons themselves, was strikingly similar to that of the somatosensory system (Extended Data Fig. 16). This suggests that a primary central core, flanked by higher-order edge neurons, may be a widespread TRN motif.

Discussion

Our results imply that sensory regions of TRN have two discrete subcircuits distinguished by their structure and function (Extended Data Fig. 17). Structurally, two distinct types of TRN neurons are segregated into central and edge zones and receive inputs from different thalamocortical nuclei. Functionally, the subcircuits have different dynamics determined by the intrinsic physiology of their respective neurons and the properties of their excitatory thalamic input synapses. The TRN subcircuits appear to be tuned to the temporal characteristics of the signals they process—transient sensory signals in the primary systems and more temporally distributed signals in the higher-order ones [10,11,18,22].

A longstanding hypothesis is that the TRN serves as a gatekeeper of forebrain information flow, permitting distinct thalamocortical circuits to regulate one another and enabling functions such as selective attention[1,5,9,34]. It has been proposed that inhibitory cross-talk between thalamic circuits[33,35] may underlie some of this regulation[8,36,37]. However, the sharp and reciprocal segregation of subcircuits we observed suggests that intrathalamic cross-talk may play a minor role. Instead, cross-system regulation in the thalamus could be mediated by other means, including descending cortical control of reticulothalamic subcircuits[2,38-40], the nature of which is only beginning to emerge[41].

The distinct kinetic features of the parallel TRN subsystems suggest that signals arriving in the thalamus will be filtered through a variety of circuit-specific temporal tuning mechanisms. For example, it has long been thought that TRN neurons undergo shifts from bursting to tonic spiking

mode as animals transition between behavioral states of quiescence and aroused wakefulness[1,23,25,27], due to activity-dependent changes in TRN cell membrane potentials and neuromodulatory tone[2,6,24,26,29,42]. Our results imply that such state transitions alter spike mode in primary/central TRN cells much more strongly than in higher-order/edge cells[28,32]. This, and the other kinetic differences between TRN subcircuits we describe, likely have profound effects for thalamic processing of afferent signals[5], including signals descending from the cortex[39].

Previous studies of several species and sensory systems have suggested separate TRN laminae for primary and higher-order connections[1,7,8], generally with just a single higher-order layer[16,33,43,44]. In contrast, in the somatosensory TRN of the mouse, we observed a primary core of CB cells surrounded by a higher-order shell-like zone of SOM cells. In at least one respect, this mouse subcircuit organization is strikingly reminiscent of the visual TRN of the primate galago; both systems have SOM-expressing zones that receive input from higher-order thalamus, and non-SOM zones that receive primary inputs[44]. Thus the association between SOM neurons of TRN and higher-order processing may be a conserved circuit feature[45]; this, together with the association between CB expression and first-order processing, are especially exciting results because they enable powerful new strategies for probing the behavioral and perceptual functions of these distinct TRN circuits[46].

Endnotes:

Funding: This work was supported by R01 NS100016, P20 GM103645, NSF 1738633, NSFGRFP 1058262, NSF 1632738. **Contributions:** R.M-G. designed and conducted the experiments, analyzed the results, and wrote the paper. B.V. designed and conducted the experiments, analyzed the results and wrote the paper. J.B.Z. conducted experiments and analyzed the results. S.L.P. and T.R.S. conducted experiments. B.W.C. designed experiments and wrote the paper. S.J.C. designed and conducted the experiments, analyzed the results, and wrote the paper. **Competing Interests:** Authors declare no competing interests. **Data and materials availability:** Data will be made available upon request. **Further acknowledgements:** We thank Zhanyan Fu, Guoping Feng, and their associates investigating the TRN, for cooperative and stimulating interactions surrounding this project. We also thank Shane Crandall, Omar Ahmed, Frederic Pouille, Brian Theyel, and Frank (Scott) Susi for helpful discussions.

References

1 Jones, E. G. *The Thalamus*. (Cambridge University Press, 2007).

2 Sherman, S. M. & Guillery, R. W. Functional organization of thalamocortical relays. *J Neurophysiol* **76**, 1367-1395, doi:10.1152/jn.1996.76.3.1367 (1996).

3 Hirsch, J. A., Wang, X., Sommer, F. T. & Martinez, L. M. How inhibitory circuits in the thalamus serve vision. *Annu Rev Neurosci* **38**, 309-329, doi:10.1146/annurev-neuro-071013-014229 (2015).

4 Crabtree, J. W. Functional Diversity of Thalamic Reticular Subnetworks. *Front Syst Neurosci* **12**, 41, doi:10.3389/fnsys.2018.00041 (2018).

5 Halassa, M. M. & Acsady, L. Thalamic Inhibition: Diverse Sources, Diverse Scales. *Trends Neurosci* **39**, 680-693, doi:10.1016/j.tins.2016.08.001 (2016).

6 Fogerson, P. M. & Huguenard, J. R. Tapping the Brakes: Cellular and Synaptic Mechanisms that Regulate Thalamic Oscillations. *Neuron* **92**, 687-704, doi:10.1016/j.neuron.2016.10.024 (2016).

7 Guillery, R. W., Feig, S. L. & Lozsadi, D. A. Paying attention to the thalamic reticular nucleus. *Trends Neurosci* **21**, 28-32 (1998).

8 Pinault, D. The thalamic reticular nucleus: structure, function and concept. *Brain Res Brain Res Rev* **46**, 1-31, doi:10.1016/j.brainresrev.2004.04.008 (2004).

9 Crick, F. Function of the thalamic reticular complex: the searchlight hypothesis. *Proc Natl Acad Sci U S A* **81**, 4586-4590 (1984).

10 Diamond, M. E., von Heimendahl, M., Knutsen, P. M., Kleinfeld, D. & Ahissar, E. 'Where' and 'what' in the whisker sensorimotor system. *Nat Rev Neurosci* **9**, 601-612, doi:10.1038/nrn2411 (2008).

11 Mease, R. A., Sumser, A., Sakmann, B. & Groh, A. Cortical Dependence of Whisker Responses in Posterior Medial Thalamus In Vivo. *Cereb Cortex* **26**, 3534-3543, doi:10.1093/cercor/bhw144 (2016).

12 Sherman, S. M. Thalamus plays a central role in ongoing cortical functioning. *Nat Neurosci* **19**, 533-541, doi:10.1038/nn.4269 (2016).

13 Fishell, G. & Rudy, B. Mechanisms of inhibition within the telencephalon: "where the wild things are". *Annu Rev Neurosci* **34**, 535-567, doi:10.1146/annurev-neuro-061010-113717 (2011).

14 Hou, G., Smith, A. G. & Zhang, Z. W. Lack of Intrinsic GABAergic Connections in the Thalamic Reticular Nucleus of the Mouse. *J Neurosci* **36**, 7246-7252, doi:10.1523/JNEUROSCI.0607-16.2016 (2016).

15 Hu, H., Cavendish, J. Z. & Agmon, A. Not all that glitters is gold: off-target recombination in the somatostatin-IRES-Cre mouse line labels a subset of fast-spiking interneurons. *Front Neural Circuits* **7**, 195, doi:10.3389/fncir.2013.00195 (2013).

16 Lam, Y. W. & Sherman, S. M. Functional organization of the thalamic input to the thalamic reticular nucleus. *J Neurosci* **31**, 6791-6799, doi:10.1523/JNEUROSCI.3073-10.2011 (2011).

17 Lee, S. H., Govindaiah, G. & Cox, C. L. Heterogeneity of firing properties among rat thalamic reticular nucleus neurons. *J Physiol* **582**, 195-208, doi:10.1113/jphysiol.2007.134254 (2007).

18 Diamond, M. E., Armstrong-James, M. & Ebner, F. F. Somatic sensory responses in the rostral sector of the posterior group (POm) and in the ventral posterior medial nucleus (VPM) of the rat thalamus. *J Comp Neurol* **318**, 462-476, doi:10.1002/cne.903180410 (1992).

19 Roth, M. M. *et al.* Thalamic nuclei convey diverse contextual information to layer 1 of visual cortex. *Nat Neurosci* **19**, 299-307, doi:10.1038/nn.4197 (2016).
20 Mease, R. A., Metz, M. & Groh, A. Cortical Sensory Responses Are Enhanced by the Higher-Order Thalamus. *Cell Rep* **14**, 208-215, doi:10.1016/j.celrep.2015.12.026 (2016).
21 Audette, N. J., Bernhard, S. M., Ray, A., Stewart, L. T. & Barth, A. L. Rapid Plasticity of Higher-Order Thalamocortical Inputs during Sensory Learning. *Neuron* **103**, 277-291 e274, doi:10.1016/j.neuron.2019.04.037 (2019).
22 Zhang, W. & Bruno, R. M. High-order thalamic inputs to primary somatosensory cortex are stronger and longer lasting than cortical inputs. *Elife* **8**, doi:10.7554/eLife.44158 (2019).
23 Steriade, M., Domich, L. & Oakson, G. Reticularis thalami neurons revisited: activity changes during shifts in states of vigilance. *J Neurosci* **6**, 68-81 (1986).
24 McCormick, D. A. & Bal, T. Sleep and arousal: thalamocortical mechanisms. *Annu Rev Neurosci* **20**, 185-215, doi:10.1146/annurev.neuro.20.1.185 (1997).
25 Marlinski, V. & Beloozerova, I. N. Burst firing of neurons in the thalamic reticular nucleus during locomotion. *J Neurophysiol* **112**, 181-192, doi:10.1152/jn.00366.2013 (2014).
26 Whitmire, C. J., Waiblinger, C., Schwarz, C. & Stanley, G. B. Information Coding through Adaptive Gating of Synchronized Thalamic Bursting. *Cell Rep* **14**, 795-807, doi:10.1016/j.celrep.2015.12.068 (2016).
27 Llinas, R. R. & Steriade, M. Bursting of thalamic neurons and states of vigilance. *J Neurophysiol* **95**, 3297-3308, doi:10.1152/jn.00166.2006 (2006).
28 Clemente-Perez, A. *et al.* Distinct Thalamic Reticular Cell Types Differentially Modulate Normal and Pathological Cortical Rhythms. *Cell Rep* **19**, 2130-2142, doi:10.1016/j.celrep.2017.05.044 (2017).
29 Destexhe, A., Contreras, D., Steriade, M., Sejnowski, T. J. & Huguenard, J. R. In vivo, in vitro, and computational analysis of dendritic calcium currents in thalamic reticular neurons. *J Neurosci* **16**, 169-185 (1996).
30 Llinas, R. & Jahnsen, H. Electrophysiology of mammalian thalamic neurones in vitro. *Nature* **297**, 406-408 (1982).
31 Lambert, R. C., Bessaih, T., Crunelli, V. & Leresche, N. The many faces of T-type calcium channels. *Pflugers Arch* **466**, 415-423, doi:10.1007/s00424-013-1353-6 (2014).
32 Kimura, A. & Imbe, H. Anatomically structured burst spiking of thalamic reticular nucleus cells: implications for distinct modulations of sensory processing in lemniscal and non-lemniscal thalamocortical loop circuitries. *Eur J Neurosci* **41**, 1276-1293, doi:10.1111/ejn.12874 (2015).
33 Pinault, D., Bourassa, J. & Deschenes, M. The axonal arborization of single thalamic reticular neurons in the somatosensory thalamus of the rat. *Eur J Neurosci* **7**, 31-40 (1995).
34 McAlonan, K., Cavanaugh, J. & Wurtz, R. H. Guarding the gateway to cortex with attention in visual thalamus. *Nature* **456**, 391-394, doi:10.1038/nature07382 (2008).
35 Lee, S. C., Patrick, S. L., Richardson, K. A. & Connors, B. W. Two functionally distinct networks of gap junction-coupled inhibitory neurons in the thalamic reticular nucleus. *J Neurosci* **34**, 13170-13182, doi:10.1523/JNEUROSCI.0562-14.2014 (2014).
36 Crabtree, J. W. & Isaac, J. T. New intrathalamic pathways allowing modality-related and cross-modality switching in the dorsal thalamus. *J Neurosci* **22**, 8754-8761 (2002).
37 Kimura, A. & Imbe, H. Robust Subthreshold Cross-modal Modulation of Auditory Response by Cutaneous Electrical Stimulation in First- and Higher-order Auditory Thalamic Nuclei. *Neuroscience* **372**, 161-180, doi:10.1016/j.neuroscience.2017.12.051 (2018).
38 Briggs, F. & Usrey, W. M. Emerging views of corticothalamic function. *Curr Opin Neurobiol* **18**, 403-407, doi:10.1016/j.conb.2008.09.002 (2008).

39 Crandall, S. R., Cruikshank, S. J. & Connors, B. W. A corticothalamic switch: controlling the thalamus with dynamic synapses. *Neuron* **86**, 768-782, doi:10.1016/j.neuron.2015.03.040 (2015).
40 Wimmer, R. D. *et al.* Thalamic control of sensory selection in divided attention. *Nature* **526**, 705-709, doi:10.1038/nature15398 (2015).
41 Nakajima, M., Schmitt, L. I. & Halassa, M. M. Prefrontal Cortex Regulates Sensory Filtering through a Basal Ganglia-to-Thalamus Pathway. *Neuron* **103**, 445-458 e410, doi:10.1016/j.neuron.2019.05.026 (2019).
42 Beierlein, M. Synaptic mechanisms underlying cholinergic control of thalamic reticular nucleus neurons. *J Physiol* **592**, 4137-4145, doi:10.1113/jphysiol.2014.277376 (2014).
43 Conley, M., Kupersmith, A. C. & Diamond, I. T. The Organization of Projections from Subdivisions of the Auditory Cortex and Thalamus to the Auditory Sector of the Thalamic Reticular Nucleus in Galago. *Eur J Neurosci* **3**, 1089-1103 (1991).
44 Conley, M., Schmechel, D. E. & Diamond, I. T. Differential Distribution of Somatostatin-like Immunoreactivity in the Visual Sector of the Thalamic Reticular Nucleus in Galago. *Eur J Neurosci* **3**, 237-242 (1991).
45 Graybiel, A. M. & Elde, R. P. Somatostatin-like immunoreactivity characterizes neurons of the nucleus reticularis thalami in the cat and monkey. *J Neurosci* **3**, 1308-1321 (1983).
46 Daigle, T. L. *et al.* A Suite of Transgenic Driver and Reporter Mouse Lines with Enhanced Brain-Cell-Type Targeting and Functionality. *Cell* **174**, 465-480 e422, doi:10.1016/j.cell.2018.06.035 (2018).

Figure 1

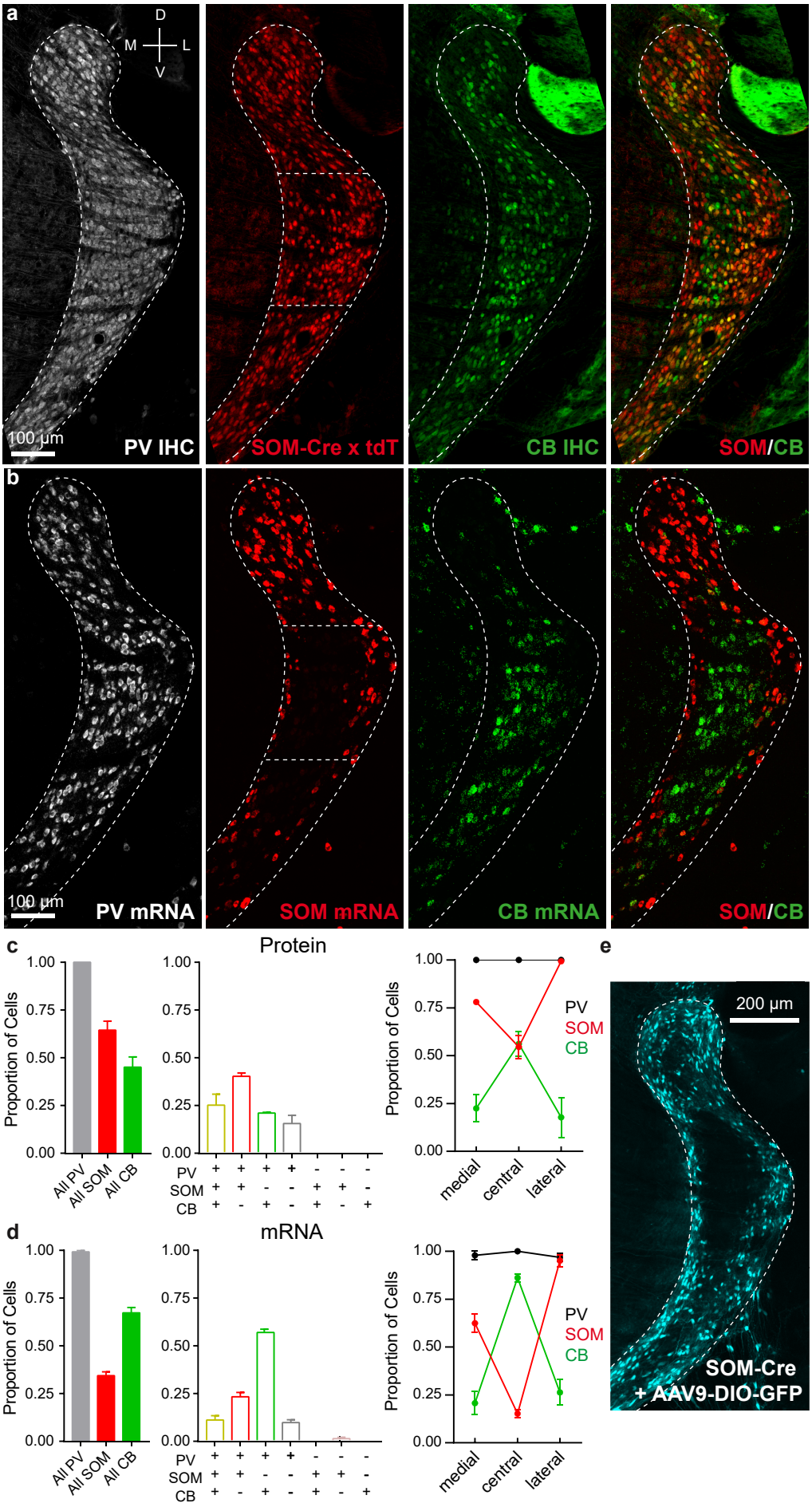
a
D
M
L
V
100 µm
PV IHC
SOM-Cre x tdT
CB IHC
SOM/CB
b
100 µm
PV mRNA
SOM mRNA
CB mRNA
SOM/CB
c
Protein
Proportion of Cells
1.00
0.75
0.50
0.25
0.00
All PV
All SOM
All CB
PV
SOM
CB
medial
central
lateral
d
mRNA
e
200 µm
SOM-Cre
+ AAV9-DIO-GFP

Figure 1. Somatosensory TRN is composed of neurochemically distinct neuron types located in separate zones.

a, Confocal images of a 40 µm section (thalamocortical plane), centered on somatosensory TRN, from a SOM-Cre x tdTomato mouse. Tissue was stained immunohistochemically (IHC) for Parvalbumin (PV) and Calbindin (CB). Somatostatin-Cre cells were genetically labeled with tdTomato (SOM-Cre x tdT). TRN outlines are based on PV labeling.

b, Confocal images of an 18 µm section (thalamocortical plane) from a WT mouse, again centered on somatosensory TRN, showing FISH expression of *Pvalb*, *Calb1* and *Sst* (named in figure as PV, CB, and SOM, respectively).

c, Left, proportion of cells expressing PV, SOM-Cre x tdT, or CB in somatosensory TRN. Middle, proportion of cells expressing combinations of the markers (n=1075 cells, n=3 sections, n=3 mice). Cells were counted in a region centered on somatosensory TRN extending 300 µm along the dorsal-ventral axis of the nucleus (dorsal-ventral boundaries indicated by horizontal lines in the SOM panels of a & b). This region consistently received axonal projections from S1 cortex (data not shown), VP, and POM thalamus (Fig. 2, Extended Data Figs. 6-7). Right, proportion of cells expressing SOM-Cre x tdT, CB, or PV for each of the 3 zones of somatosensory TRN. Of the 1075 cells counted, 187 were in the medial zone (medial 20%), 746 in the central zone (central 60%), and 142 in the lateral zone (lateral 20%). Fractional SOM-Cre x tdT cell densities were higher in the edge zones than the central zone, whereas fractional CB cell densities were higher in the central than the edge zones (all $P < 0.001$, Chi-square test with Yates' correction).

d, Same as (c) but for mRNA (n=593 cells, n=6 sections, n=6 mice). Right, of the 593 cells counted, 98 were in the medial zone, 412 in the central zone, and 83 were in the lateral zone. Again, both SOM and CB cells were differentially distributed across zones ($P < 0.001$, Chi-square test with Yates' correction).

e, Confocal image of a 90 µm slice from a P23 SOM-Cre mouse. AAV9-DIO-GFP was stereotactically injected in TRN at P14 and GFP (shown in cyan) was expressed in cells that were Cre-positive on or after the day of injection.

Figure 2

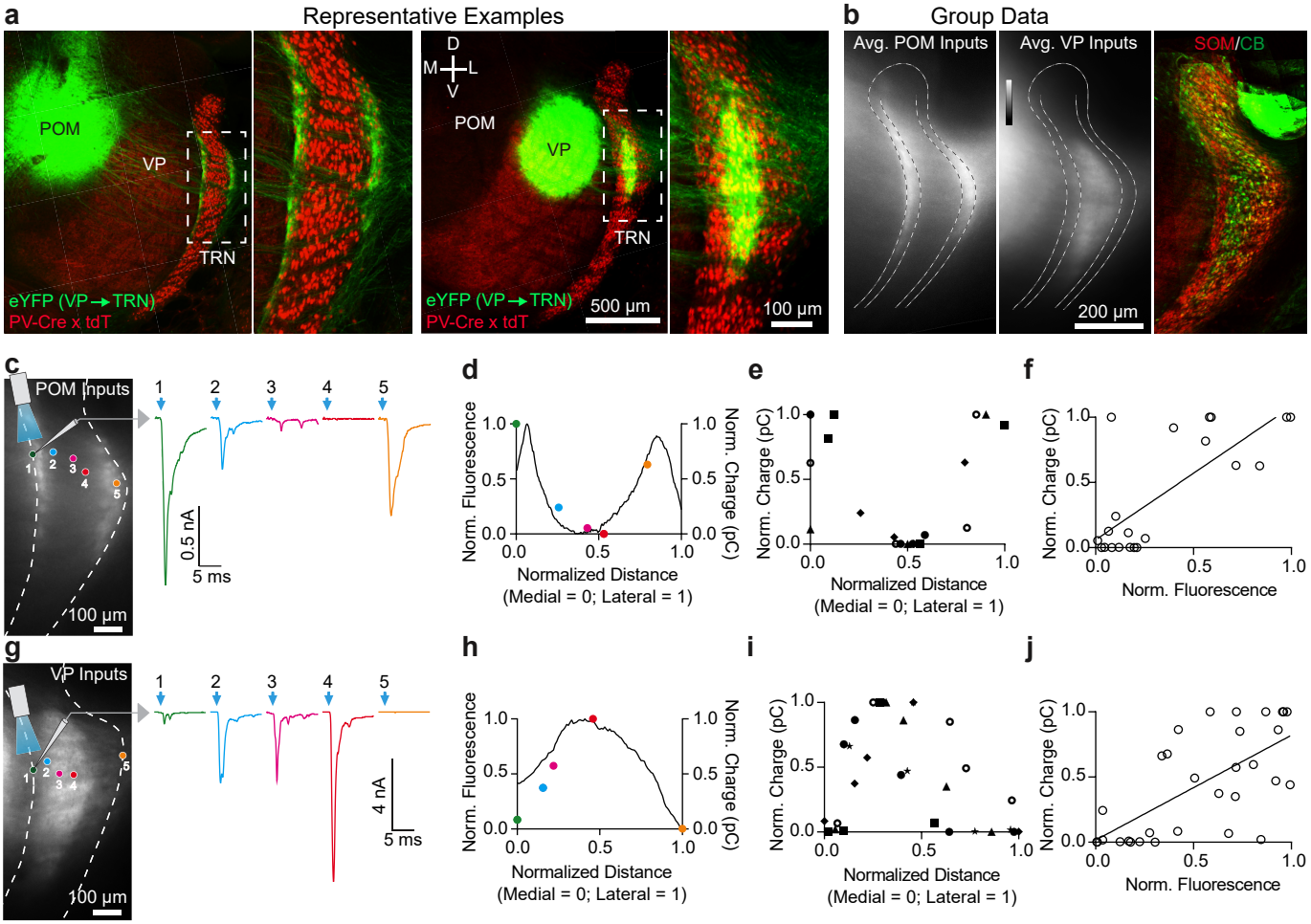
a
Representative Examples
POM
VP
TRN
eYFP (VP→TRN)
PV-Cre x tdT
D
M
L
V
500 µm
100 µm
b
Group Data
Avg. POM Inputs
Avg. VP Inputs
SOM/CB
200 µm
c
POM Inputs
1
2
3
4
5
0.5 nA
5 ms
100 µm
d
Norm. Fluorescence
Norm. Charge (pC)
Normalized Distance
(Medial = 0; Lateral = 1)
e
Norm. Charge (pC)
Normalized Distance
(Medial = 0; Lateral = 1)
f
Norm. Charge (pC)
Norm. Fluorescence
g
VP Inputs
4 nA
5 ms
100 µm
h
Norm. Fluorescence
Norm. Charge (pC)
Normalized Distance
(Medial = 0; Lateral = 1)
i
Norm. Charge (pC)
Normalized Distance
(Medial = 0; Lateral = 1)
j
Norm. Charge (pC)
Norm. Fluorescence

Figure 2. VP, a first-order thalamic nucleus, targets the central zone of somatosensory TRN, whereas POM, a higher-order nucleus, targets the edges of TRN.

a, Representative confocal images (40 µm sections in the somatosensory thalamocortical plane) illustrating the distinct projection patterns from POM and VP to TRN. AAV2-hSyn-ChR2-eYFP was stereotactically injected in POM (left) or VP (right) and characteristic anterograde projections to the edges and center of TRN were observed, respectively. Red: PV-Cre x tdT. Green: ChR2-eYFP.

b, Group data showing average thalamic projections to TRN. Viral anterograde tracing was conducted as in the experiments of panel a. Left, POM afferents targeted the medial and lateral edges of somatosensory TRN (average of n=9 slices from 9 mice). Middle, VP inputs preferentially targeted the central zone of somatosensory TRN (average of n=8 slices from 8 mice). Central/edge boundaries were drawn at 20% and 80% of the medial-lateral distance across the TRN. For each slice, the TRN was first outlined using either tdTomato expression driven by SOM-Cre (n=6 for POM, n=4 for VP) or bright field images (n=3 for POM, n=4 for VPM), then those outlines were used to warp the slices to a common reference TRN, allowing precise alignment across mice for averaging (see extended methods). Additional individual POM and VP injections and projections are shown in Extended Data Figs. 7-8). Right, Average SOM and CB immunohistochemical profiles (n=5 sections from 5 mice) aligned to the same reference TRN as the average anterograde projection maps.

c, Synaptic responses to activation of the POM axons were recorded from cells across the mediolateral axis of somatosensory TRN to test how synaptic strength relates to anterograde fluorescence intensity and topographical location. Left, live image of a 300 µm slice containing TRN (outlined) following ChR2-eYFP expression in POM neurons. Each colored circle represents the location of a patched TRN cell. The TRN outline was generated using the SOM-Cre tdT expression. Right, EPSCs evoked in TRN cells by optical activation of POM axons (each trace is an average of 10 sweeps, -84 mV). Trace colors match cell locations shown in the left image and in panel (d). Arrows indicate onset of LED flashes (1 ms durations).

d, Normalized fluorescence intensity (black line, left axis) and synaptic charge (colored dots, right axis) for the cells in (c), plotted as a function of cells' medial-lateral positions in TRN. Fluorescence was normalized to the maximum and minimum levels across somatosensory TRN and synaptic responses were normalized to the strongest EPSC recorded in the slice.

e, Relationship between soma location in TRN and evoked synaptic response (n=21 cells from 5 preps, each prep represented by a unique symbol shape, a minimum of 3 cells were recorded per

prep). Somas close to the medial and lateral edges of TRN responded strongly to POM input and those in the center had minimal POM inputs.

f, TRN cells' synaptic responses to POM input (normalized charge) and the normalized fluorescence intensity from POM axons surrounding the cell were correlated ($r=0.75$, $p<0.0001$, Pearson's coefficient).

g-h, Synaptic responses of TRN cells to activation of VP axons. Same as (c-d) but ChR2-eYFP was expressed in VP neurons and projections.

i, Relationship between soma location in TRN and evoked synaptic responses ($n=31$ cells from 6 preps, a minimum of 5 cells were patched per prep) shows that the somas close to the center of TRN respond strongly to VP input and those in medial and lateral edges respond weakly.

j, TRN cell's normalized synaptic charge after activation of VP axons and the anterograde fluorescence from VP surrounding the cell were correlated ($r=0.68$, $p<0.0001$, Pearson's coefficient).

Figure 3

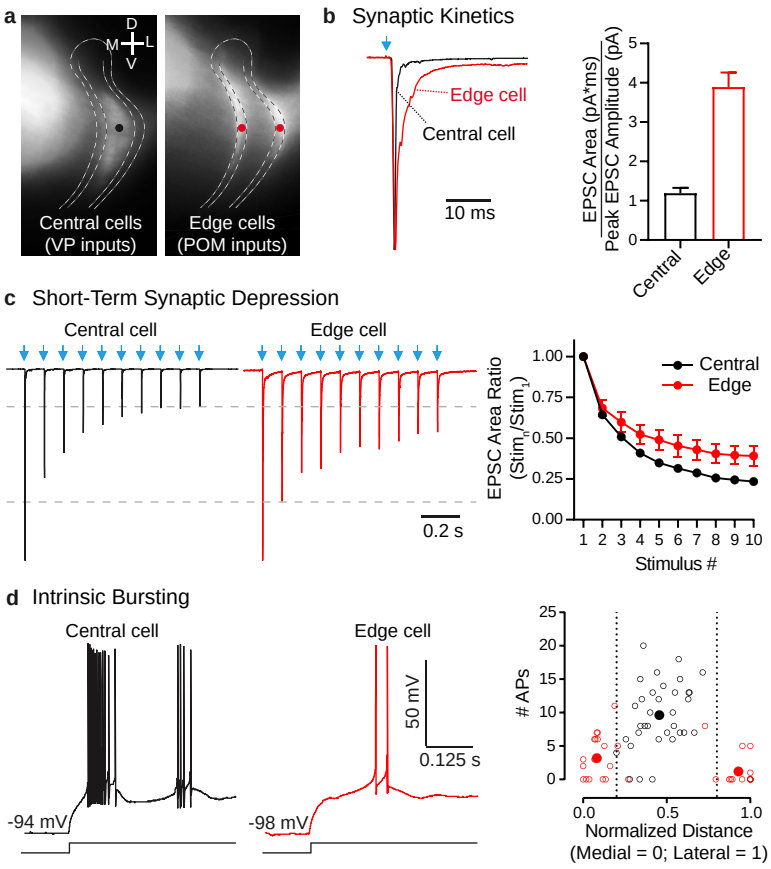
a
D
M
L
V
Central cells
(VP inputs)
Edge cells
(POM inputs)
b Synaptic Kinetics
Edge cell
Central cell
10 ms
EPSC Area (pA*ms)
Peak EPSC Amplitude (pA)
Central
Edge
c Short-Term Synaptic Depression
Central cell
Edge cell
0.2 s
EPSC Area Ratio
(Stim$_n$/Stim$_1$)
Central
Edge
Stimulus #
d Intrinsic Bursting
Central cell
Edge cell
50 mV
0.125 s
-94 mV
-98 mV
APs
Normalized Distance
(Medial = 0; Lateral = 1)

Figure 3. Central and edge TRN cells receive thalamic inputs with different kinetics and synaptic depression, and have distinctly different bursting tendencies

a, Schematic showing locations of TRN somas targeted by VP inputs (black dot) and POM inputs (red dots).

b, POM-evoked EPSCs from edge cells are more prolonged than VP-evoked EPSCs from central cells. Left, representative traces showing optogenetically evoked EPSCs (stimulus 1 of (c)) for example cells of each type, normalized to their peak amplitudes. Holding potential was -84 mV. Right, POM-evoked edge cell responses have greater fractional area in the later stages of the EPSCs (quantified as the ratio of the area to the peak amplitude; $p<0.0001$, unpaired t-test, two tailed; central = 42 cells from 7 mice; edge = 14 cells from 7 mice).

c, Left, short-term synaptic depression of evoked EPSCs from VP to central cells and from POM to edge cells (representative traces; 10 Hz LED trains, 1 ms per stimulus; arrows indicate stimuli). Traces were normalized to the peak of the first stimulus. Right, average synaptic depression (same cells as for panel (b)). Light intensities were adjusted to evoke ~ 1.5 nA peak responses (average LED powers: 19.7 mW for POM, 5.2 mW for VP). EPSC areas measured over the first 10 ms of each response. There was greater short-term depression for the central cells (VP inputs) than the edge cells (POM inputs) ($p < 0.0001$, ANOVA stim. 2-10; All $p < 0.005$ from stimulus 5-10, Bonferroni's t-test).

d, Left, intrinsic bursting of central and edge cells (representative traces). Cells were injected with negative intracellular current to produce a steady state V_m of ~-95 mV, then the current was abruptly removed to trigger "offset bursts". Right, number of action potentials per burst for central cells (black) and edge cells (red) as a function of medial-lateral soma position in the TRN (medial edge = 0, lateral edge = 1). Open circles show individual cell measurements; filled circles show averages for cells in central and edge zones. Average action potentials per offset burst were 9.6 ± 0.69 for central cells (n=34 from 11 mice), 3.2 ± 0.70 for medial cells (n=22 cells from 10 mice), and 1.2 ± 0.50 for lateral cells (n=16 from 10 mice). Edge cells discharged far fewer action potentials per burst than central cells (unpaired t-test, two-tailed, $p<0.0001$).

Figure 4

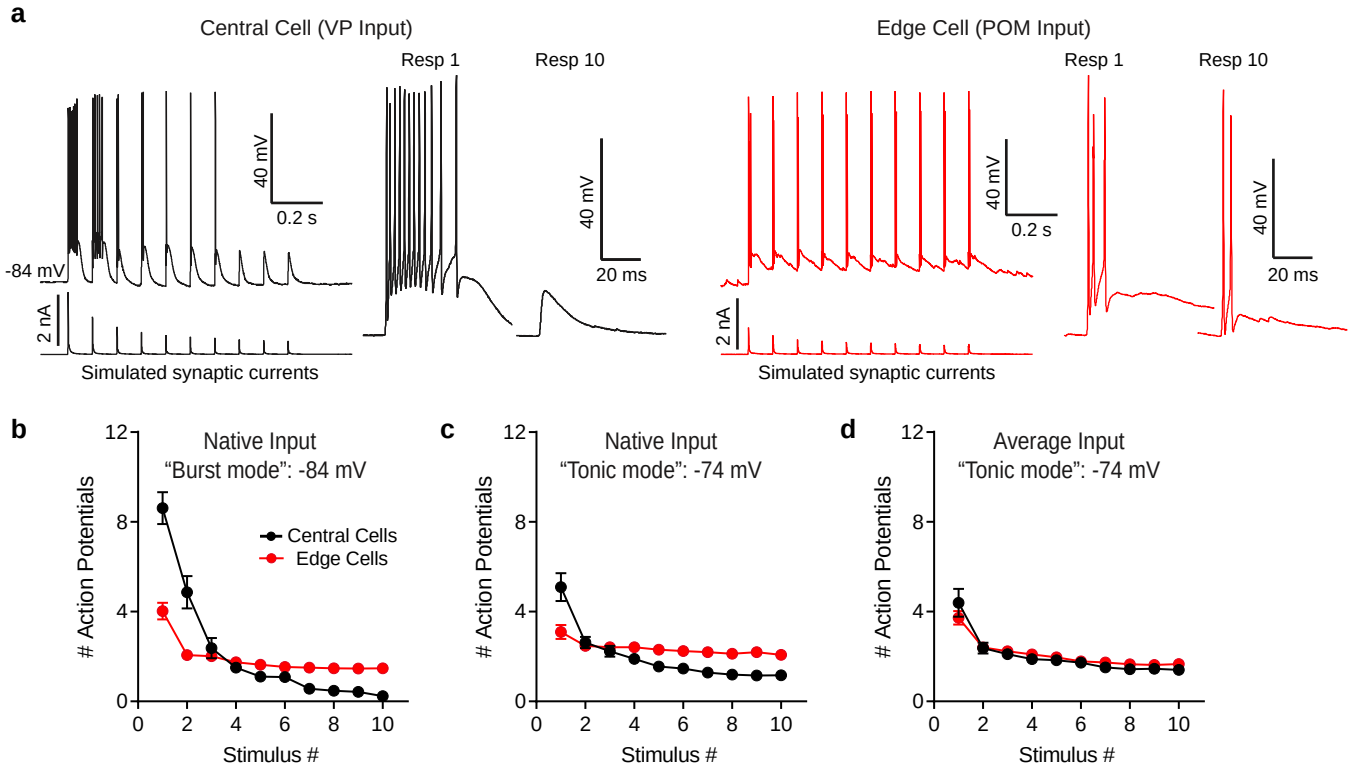
a
Central Cell (VP Input)
Resp 1
Resp 10
40 mV
0.2 s
-84 mV
2 nA
Simulated synaptic currents
40 mV
20 ms
Edge Cell (POM Input)
Resp 1
Resp 10
40 mV
0.2 s
2 nA
Simulated synaptic currents
40 mV
20 ms
b
Native Input
"Burst mode": -84 mV
Central Cells
Edge Cells
Action Potentials
Stimulus #
c
Native Input
"Tonic mode": -74 mV
Action Potentials
Stimulus #
d
Average Input
"Tonic mode": -74 mV
Action Potentials
Stimulus #

Figure 4. Thalamus-evoked spiking in central TRN cells is transient whereas TRN edge cell responses are more sustained

a, Simulated synaptic currents were modeled on VP and POM inputs to TRN cells by averaging the previously recorded EPSCs evoked in central and edge TRN cells with 10 Hz photostimulation of the respective pathways (EPSC data from Fig. 3). Simulated VP and POM synaptic currents were set to have equal total charge across the full one-second waveform (49.5 pC). Left (black), response of a central cell (top) to simulated VP synaptic currents. The first stimulus in the 10 Hz train evoked a burst of 12 action potentials (APs), but responses depressed to zero by stimulus 8. Right (red), spike responses of an edge cell to simulated POM synaptic currents. The first stimulus evoked 3 APs, and spike responses persisted during repetitive stimulation (stimulus 10 evoked 2 APs).

b, Population data showing spike output of central cells to simulated VP currents (i.e., their native synaptic input) and edge cells to their native simulated POM input. The TRN cells were held in 'burst-mode' (-84 mV) using direct current if necessary (13 central cells, 11 edge cells from 8 mice). Central cell responses were initially strong and depressed sharply whereas edge cell responses were more stable (# of AP counts from stimulus 1 to stimulus 10 declined by 97% for central cells and 63% for edge cells; $p<0.0001$, t-test, unpaired, two-tailed).

c, Same as panel (b) except cells were held in 'tonic-mode' (-74 mV) to reduce influences of intrinsic bursting. (13 central cells, 11 edge cells from 8 mice). This caused the central cell response patterns to become more like the edge responses, but significant differences remained (# of AP counts from stimulus 1 to stimulus 10 declined by 77% for central vs 33% for edge cells, $p=0.0002$, t-test, unpaired, two-tailed).

d, Population data showing the spike output of central and edge cells in response to identical simulated synaptic currents (average of VP- and POM-simulated EPSCs). The recorded TRN cells were held in 'tonic-mode' (-74 mV; 13 central cells, 11 edge cells from 8 mice). The APs response patterns of the central and edge cells did not differ ($p=0.2$, t-test, unpaired, two-tailed).

Extended Data Figure 1

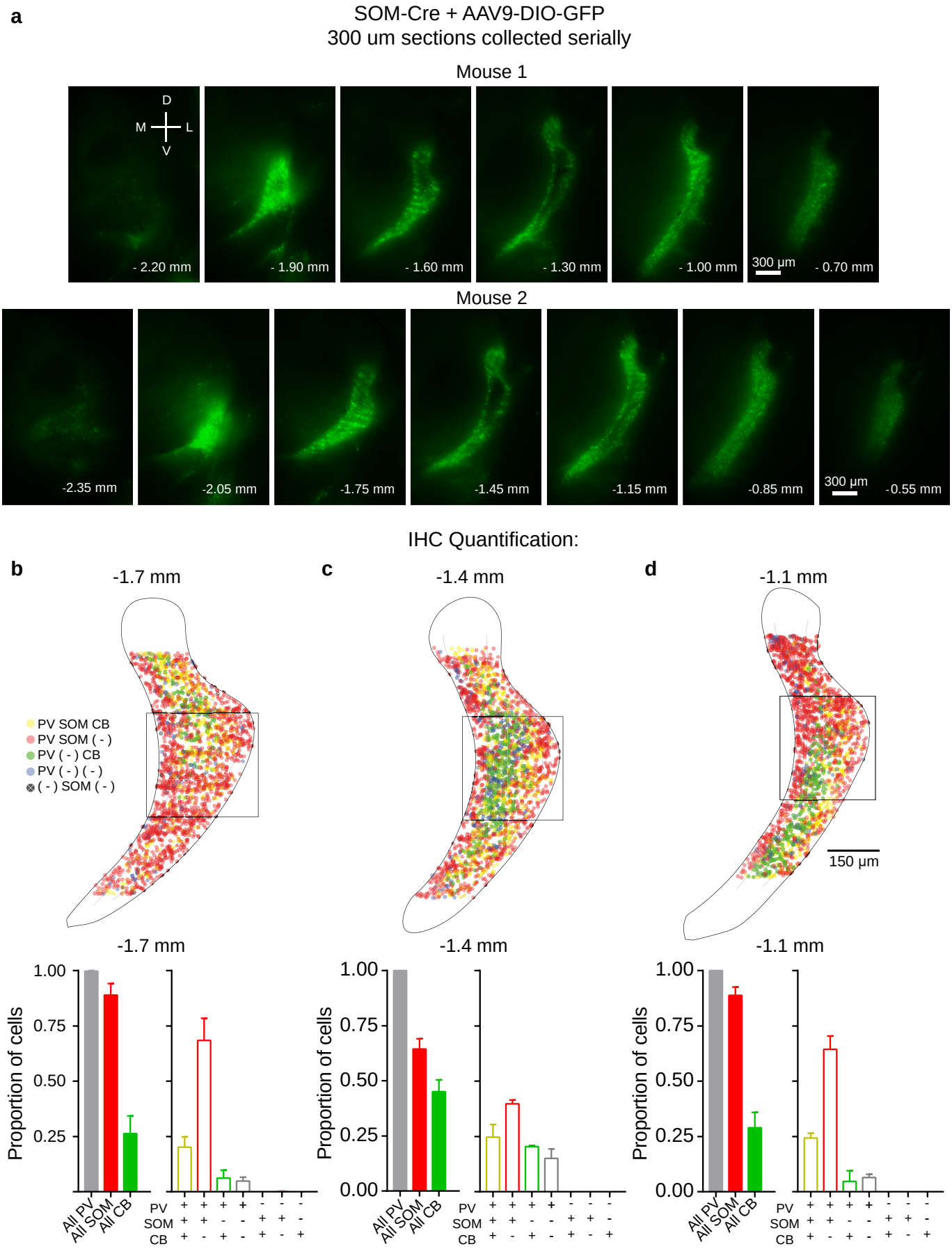

Extended Data Figure 1. Somatostatin-expressing cells form a shell-like structure surrounding a central core of somatosensory TRN

a, Epifluorescence images showing live 300 µm-thick serial sections expressing AAV9-DIO-GFP (9 days of expression) through the TRN of two P23 SOM-Cre mice. Sections show anterior-posterior position relative to bregma. Notice how the SOM-sparse core of somatosensory TRN (centered ~ -1.4 mm from Bregma) is surrounded on all sides by a shell of SOM-Cre expressing cells.

b-d, Top, dot plots showing the locations of the genetically or immunohistochemically labeled TRN cell types for sections centered at -1.7, -1.4 and -1.1 mm from Bregma. Cell positions and counts were determined from 40 µm thick sections imaged on a confocal microscope (3 sections from 3 different mice for each slice plane). Images for a given plane were aligned to a common reference image using BUnwarpJ, facilitating accurate comparisons of cell positions across mice (see Methods). Bottom, proportion of cells expressing PV, CB, SOM-Cre x tdT, and combinations of the markers. Quantification was restricted to the 300-µm boxed regions shown in the top panels. Total cell counts: b= 947 c= 1075, d = 843. The proportion of CB cells was highest in the middle section of somatosensory TRN (-1.4 mm), whereas the proportion of SOM-Cre x tdT cells was lowest in the middle section and higher in the more anterior and posterior sections ($P < 0.001$, Chi-square test with Yates' correction).

Extended Data Figure 2

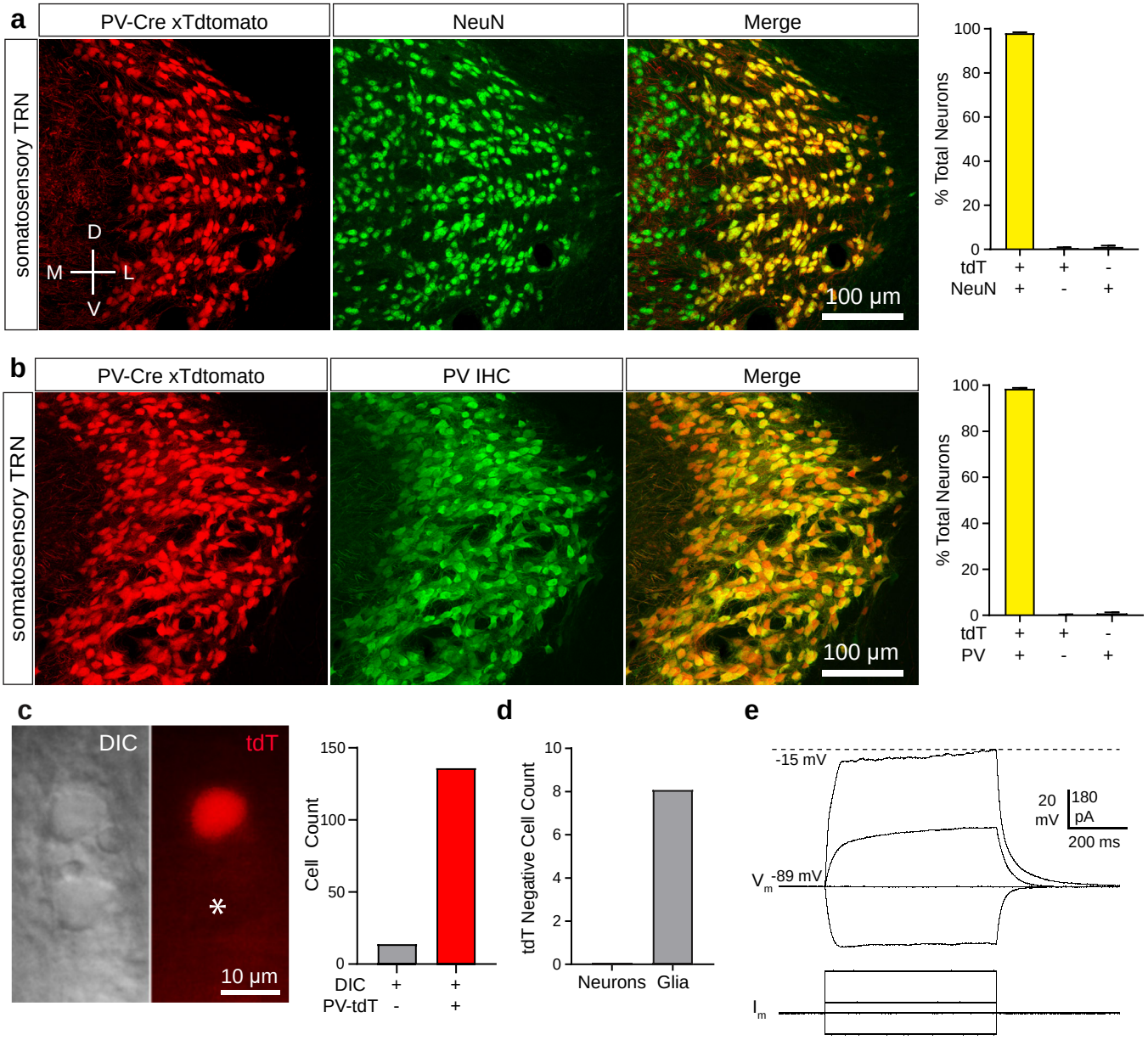

Extended Data Figure 2. Nearly all somatosensory TRN neurons express parvalbumin.

a, Left, confocal images of the somatosensory sector of TRN in a PV-Cre x tdTomato mouse stained immunohistochemically for NeuN (tdT shown as red, NeuN as green). Right, quantification of expression. In PV-Cre x tdTomato mice, 98.09% of TRN neurons were positive for both tdTomato and NeuN, 0.73% were positive for tdTomato but negative for NeuN, and 1.18% were negative for tdTomato and positive for NeuN (1218 neurons, 2 sections, 1 mouse).

b, Same as (a) but tissue was stained immunohistochemically for Parvalbumin. In PV-Cre x tdTomato mice, 98.66% of TRN neurons were positive for tdTomato and PV, 0.34% were positive for tdTomato but negative for PV and 0.34% were negative for tdTomato and positive for NeuN (1177 neurons, 2 sections, 1 mouse).

c, DIC-IR (left) and TDT fluorescence (right) images of TRN in a live slice from a PV-Cre x Ai14 mouse. Asterisk indicates tdT non-expressing soma. During such live imaging, tdT negative somata were relatively rare in TRN (>80% of somata visualized in DIC-IR expressed tdT; n=5 slices from 3 mice; right panel).

d. All TDT-negative cells targeted for recording (n = 8/8) were found to be glia.

e. TRN glial cells had hyperpolarized resting potentials (typically < -85 mV) and no action potentials even when depolarized with large intracellular current injections.

Extended Data Figure 3

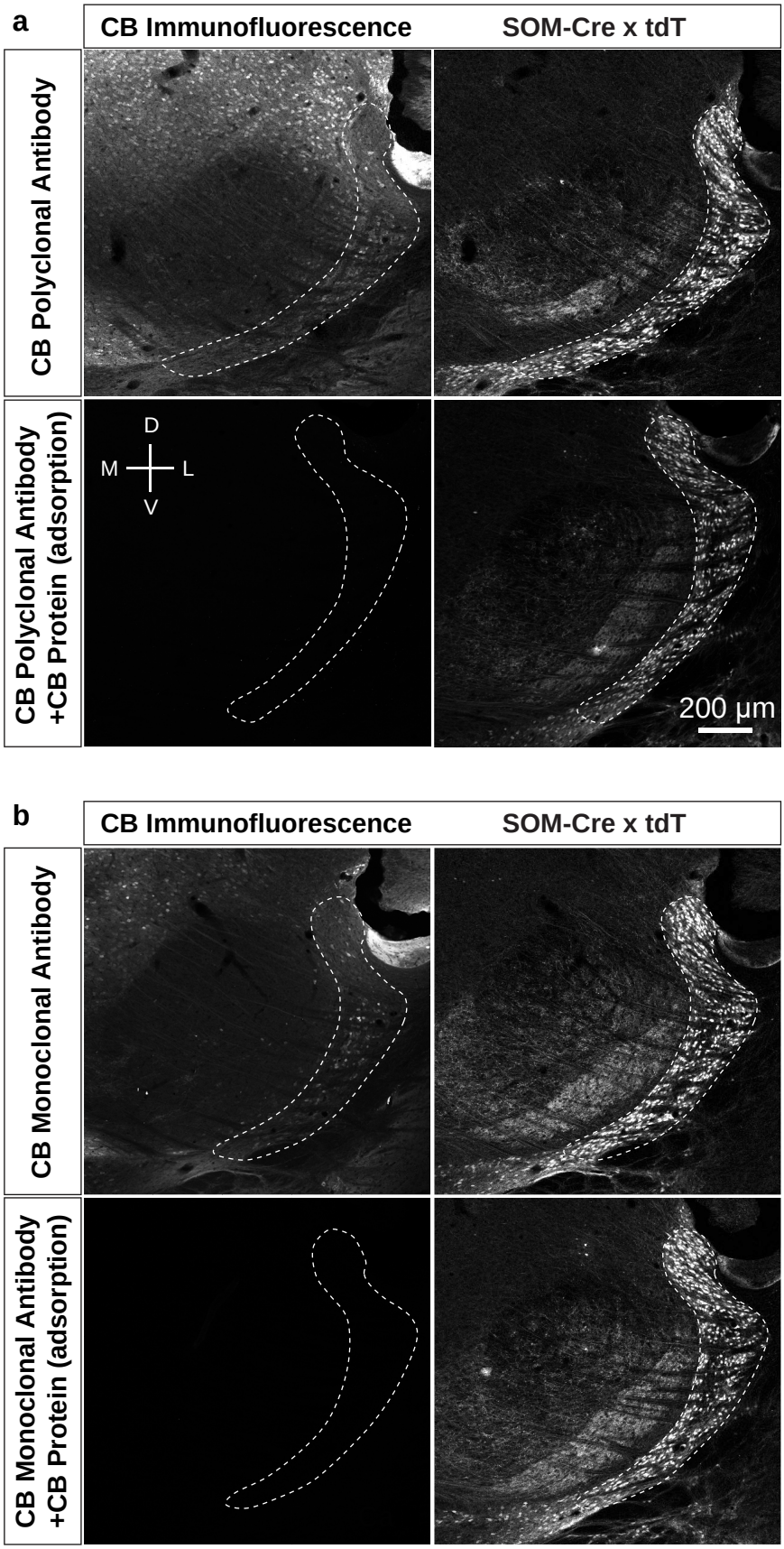

Extended Data Figure 3. The Calbindin antibody binds Calbindin protein.

a, Top, calbindin polyclonal antibody (same as Figure 1) labels cells in the central zone of TRN. Additionally, it labels cells in higher order thalamic relay nuclei, as previously described[47,48]. Bottom, adsorption assay in adjacent section. For the assay, 3.33 µg of calbindin protein was added for each 1 µL of antibody solution prior to tissue incubation. The lack of tissue labeling in the bottom panel indicates that the antibody does effectively bind calbindin protein. Images in top and bottom panels were acquired with the same confocal microscope settings (n=2 mice).

b, Same as (a) but for calbindin monoclonal antibody (n=1 mouse).

Extended Data Figure 4

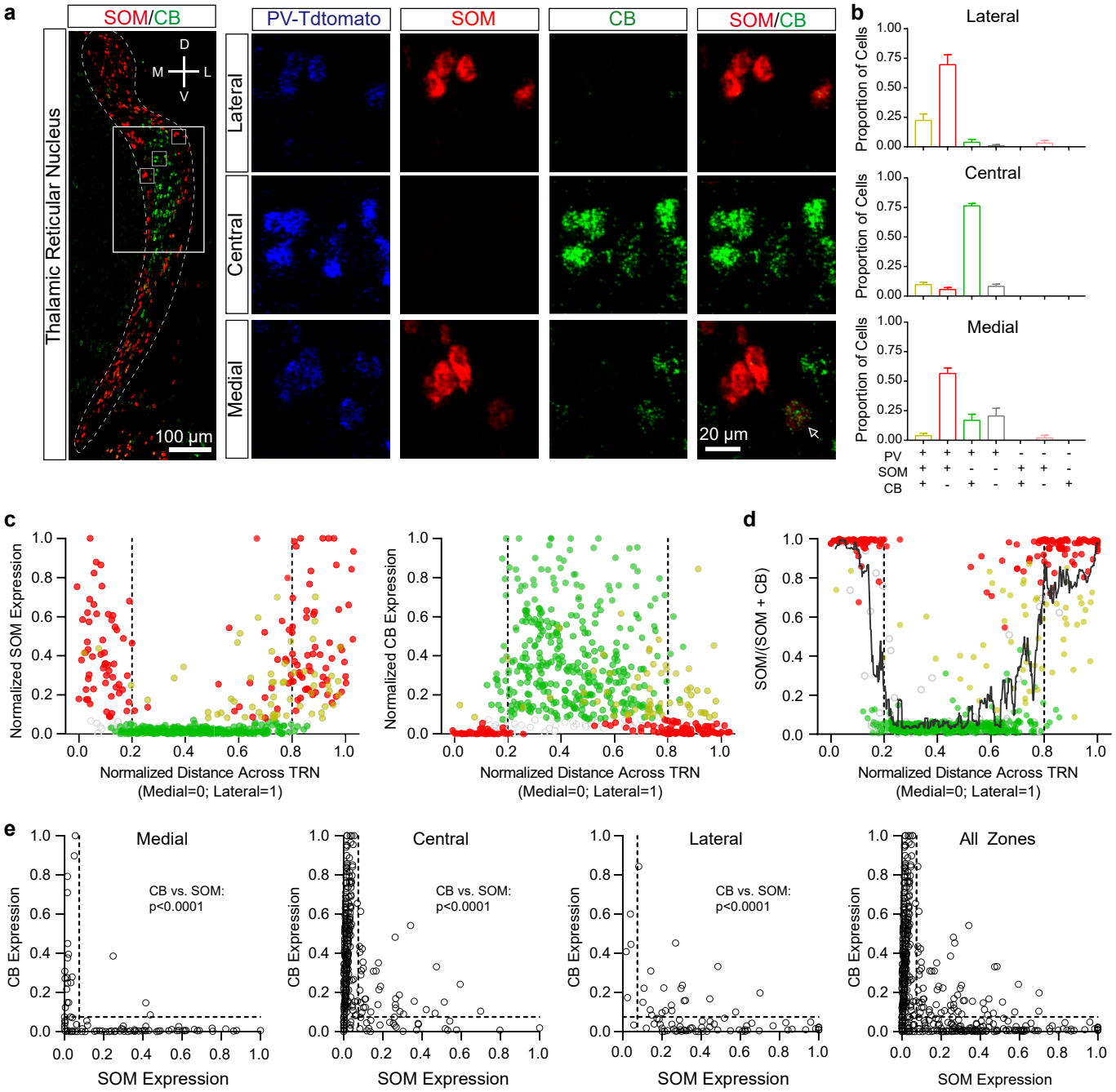

Extended Data Figure 4. Cells expressing SOM and CB mRNA are topographically segregated in somatosensory TRN.

a, Left, confocal image overlay of SOM and CB mRNA expression of an 18 µm thick section through the TRN of a P25 PV-Cre x tdT mouse. In the somatosensory sector of the TRN (300-µm boxed region), SOM expressing cells are preferentially localized in the medial and lateral edge zones, whereas CB cells are generally in the central zone. Insets show mRNA expression patterns of cells in the lateral edge (top row), central (middle row), and medial edge (bottom row) zones. Although most cells predominantly expressed either SOM (red) or CB (green) mRNA, ~10% of cells had clear expression of both (e.g., cell at arrow). Note the relatively weak fluorescence for both markers in this dual SOM-CB cell compared with those expressing just one of these markers (quantified below).

b, Proportion of cells expressing various combinations of markers for each zone. Total counts: 593 cells from 6 sections of 6 mice (average = 98.9 ± 8.5 cells/section). 99.1 ± 0.2% of cells expressed PV mRNA. Most cells in the medial and lateral edge zones express only SOM and PV, but not CB (~64**%**). In contrast, most central cells express only CB and PV, but not SOM (~76**%**).

c, Left, normalized SOM mRNA expression as a function of medial-lateral position in the TRN (0= most medial, 1= most lateral). Right, normalized CB expression as function of normalized distance. Cells expressing SOM but not CB (red) are concentrated near the medial and lateral edges (mean SOM expression for Edge vs Central zones: 0.325 ± .020 vs. 0.052 ± 0.006, $p<0.0001$, t-test). Cells in the center generally have high levels of CB but not SOM (green; mean CB expression for Central vs Edge zones: 0.326 ± 0.012 vs. 0.086 ± 0.012, $p<0.0001$, t-test). About 10% of somatosensory TRN cells express both SOM and CB (yellow). These dual SOM/CB cells cluster in the lateral half of the TRN, with their focus being near the boundary between the central and lateral zones (average normalized position on the medial-lateral axis = 0.71 ± 0.02). Compared with the cells expressing SOM or CB “alone”, the dual SOM/CB cells had lower expression of both SOM (SOM/CB cells: 0.25 ± 0.02 vs SOM only: 0.43 ± 0.02, $p<0.0001$, t-test) and CB mRNA (SOM/CB cells: 0.23 ± 0.15 vs CB only: 0.39 ± 0.01, $p<0.0001$, t-test). Together this suggests they may represent a transitional population. About 9% of somatosensory TRN cells express PV only (gray outline), and they are dispersed fairly evenly across the sector (mean position: 0.38 ± 0.03 from the medial edge).

d, Relative expression of SOM versus CB (within-cell) as a function of medial-lateral position in the TRN (a value of 1.0 on the y-axis index indicates SOM expression only, a value of 0 indicates CB only, and 0.5 indicates equal expression values for SOM and CB). Most cells (80% of the sample) have very high (>0.9) or very low (<0.1) relative expression scores, indicating most cells

have strong biases toward a single marker (10:1 ratios or greater). Consistent with Figure 1 and panels a-c here, SOM-biased cells tend to cluster toward the TRN edges, whereas CB-biased are located centrally (edge vs. central preference scores: 0.76 ± 0.03 vs. 0.14 ± 0.01, $p<0.0001$, t-test). A moving average (11-point) is superimposed to illustrate the spatial trends in expression bias. Interestingly, even the dual-expressing SOM/CB cells (yellow) tend to have a topographical preference according to relative SOM vs. CB expression: Dual-expressing edge cells tend to have higher SOM:CB preference scores than dual-expressing central cells (Dual edge vs central cells: 0.58 ± 0.04 vs. 0.47 ± 0.04, $p=0.06$, t-test).

e, CB expression as a function of SOM expression for cells in the medial, central, lateral, and combined zones. P-values are the results of paired (within-cell) t-tests comparing CB and SOM expression. SOM expression was significantly higher than CB expression for the edge cell groups, whereas the reverse was true for the central cells.

Extended Data Figure 5

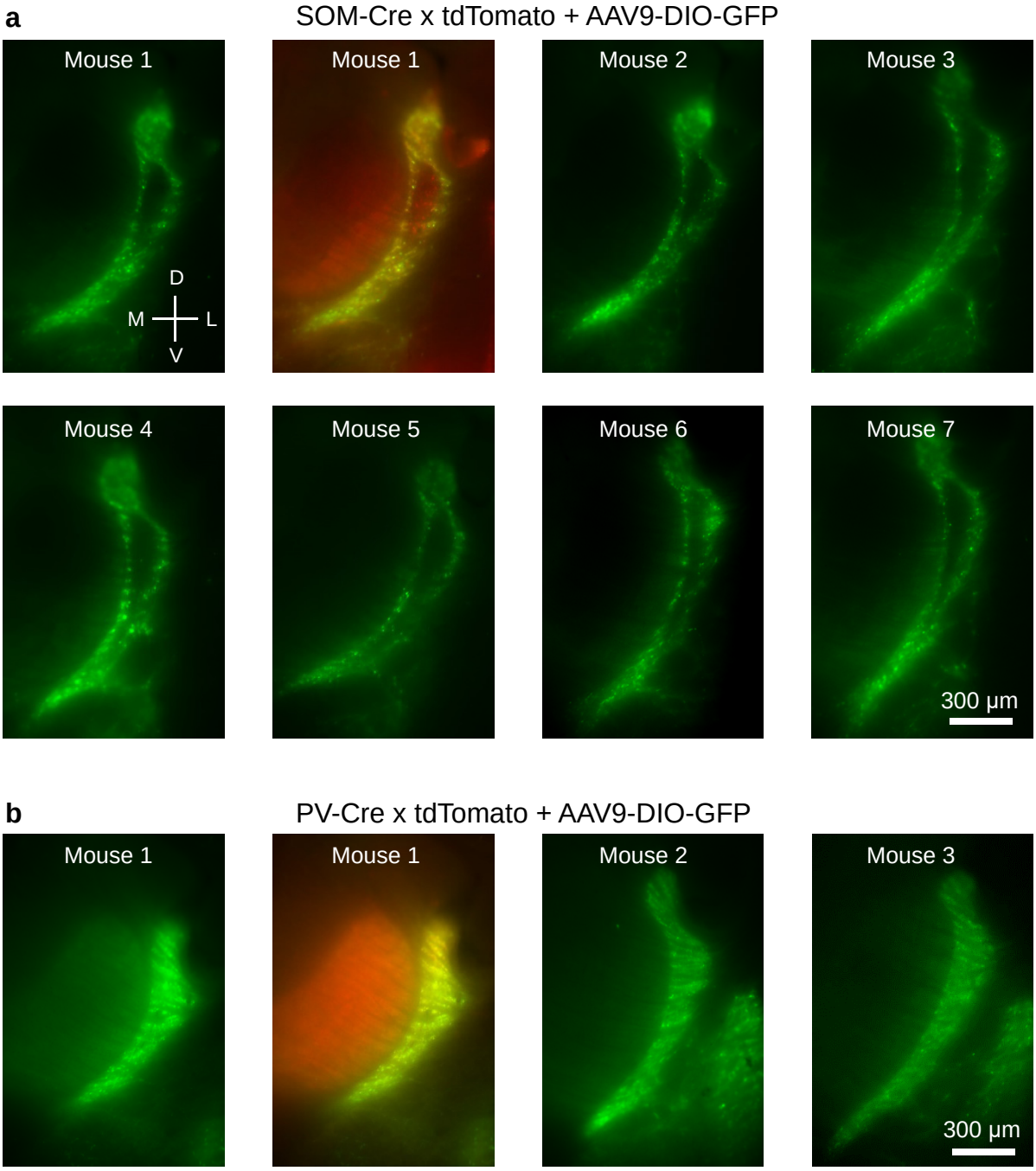

Extended Data Figure 5. Somatostatin-Cre expression is restricted to the edges of somatosensory TRN after early development.

a, Epifluorescence images of virally induced, SOM-Cre-dependent GFP expression patterns in TRN (live 300 µm thick slices from 7 mice). An AAV carrying a Cre-dependent GFP gene (AAV9-DIO-GFP) was injected throughout the TRNs of SOM-Cre x tdTomato or SOM-Cre x ICR mice. This drove GFP expression (green) in SOM cells that expressed Cre at or after the time of the virus injection (age at injection = P17.1 ± 1.18 days; age at imaging = 26.8 ± 1.19). "Mouse 1": Images of GFP alone and overlay of GFP and genetically-labeled tdTomato cells. Mouse 2-Mouse 7: GFP alone. Within the somatosensory TRN, expression of SOM-Cre X GFP is restricted to the edges of the nucleus and excluded from the central zone after early development.

b, Same as in panel (a) except using PV-Cre mice (age at virus injection = P14: age at imaging = P23). Nearly all cells express both genetically-labeled PV-Cre x tdTomato and virally-induced PV-Cre x GFP. In addition to demonstrating ubiquitous postnatal PV-Cre expression across TRN, these results show that the virus has no obvious tropisms for different topographic regions of the TRN.

Extended Data Figure 6

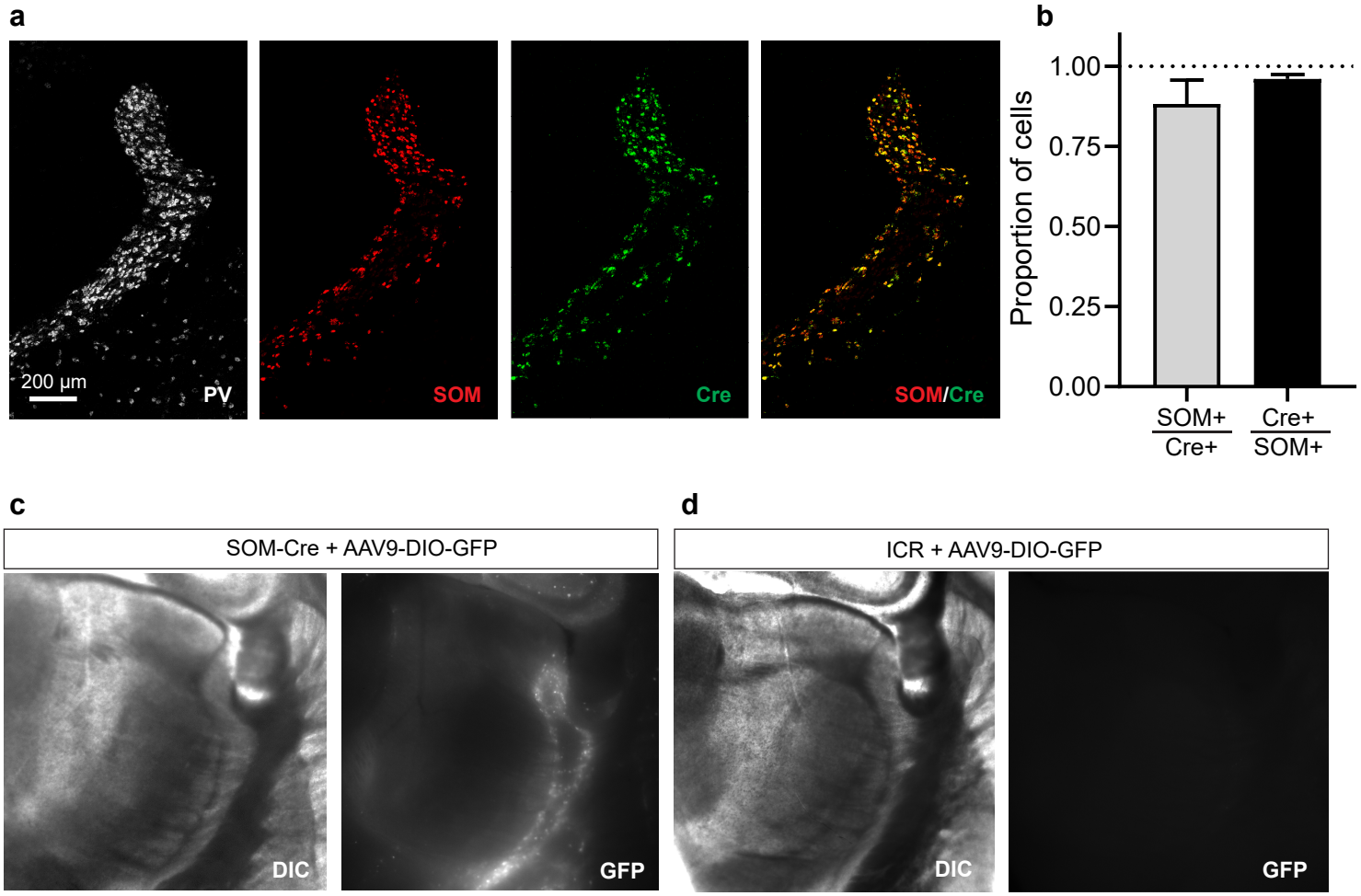

Extended Data Figure 6. Cre recombinase, and viral Cre-dependent protein expression, is restricted mainly to SOM cells in postnatal SOM-Cre mice

a, Confocal images of PV, SOM and Cre mRNA expression through the TRN of a P27 SOM-Cre heterozygous mouse (18 µm thick section). The overall patterns of SOM and Cre mRNA labeling are nearly identical.

b, SOM and Cre mRNA are generally expressed in the same neurons. Total counts: 167 cells from 5 sections of 4 mice (measured in the somatosensory sector of TRN). Of the Cre-expressing cells, 88.3 ± 0.1% expressed SOM mRNA. Of the SOM-expressing cells, 96.1 ± 0.01% expressed Cre mRNA.

c, AAV9-DIO-eGFP injections into the TRNs of postnatal SOM-Cre mice leads to eGFP expression patterns that are very similar to SOM mRNA patterns. Left, DIC and epifluorescence images from a live 300 µm-thick section expressing AAV9-DIO-GFP (9 days after virus injection) in a SOM-Cre heterozygous mouse. For additional examples see Fig. 1g, Extended Data Figs. 1a & 5.

d, Same as (c) but virus injected into a WT mouse (ICR strain; no Cre expression) (tested in n=2 mice). Matching display settings were utilized for the slices in (c) and (d). The lack of fluorescent signal indicates that the AAV-DIO-GFP virus used here drives GFP expression only in Cre-expressing cells.

Extended Data Figure 7

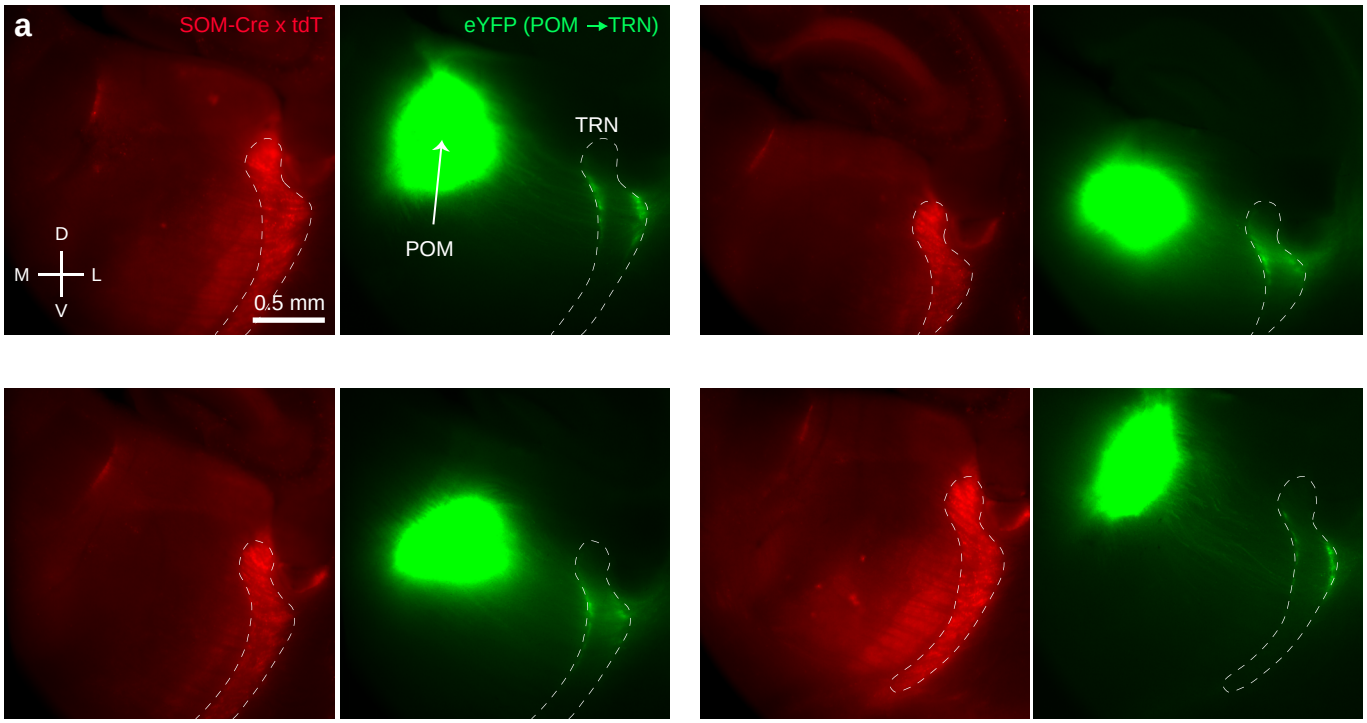

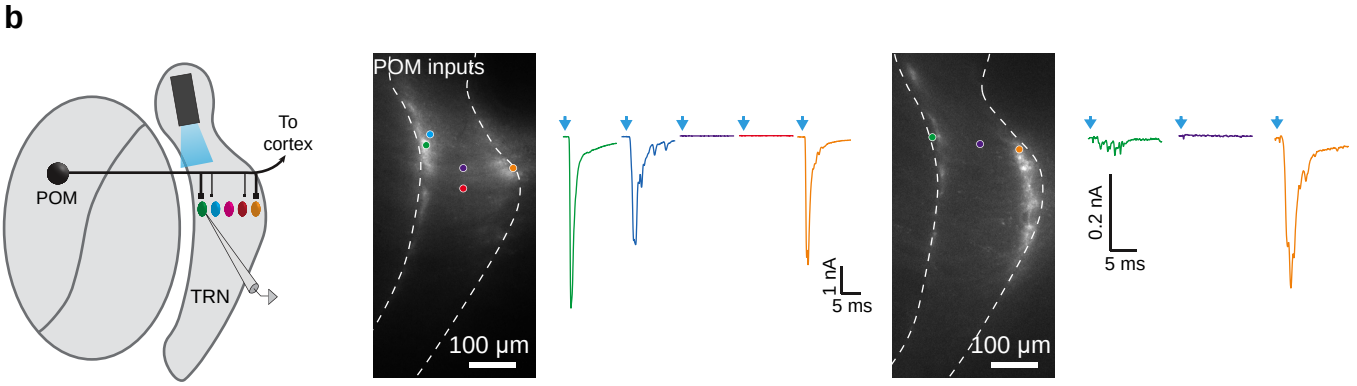

Extended Data Figure 7. POM afferents target the SOM-dense medial and lateral edges of somatosensory TRN

a, Four representative examples showing the POM injection sites and anterograde projections to TRN in live 300 µm slices. Red: SOM-Cre x tdT. Green: ChR2-eYFP. Boundaries of the thalamic nuclei (TRN outlined by dashed lines) were determined from SOM-Cre X tdT fluorescence and by brightfield images (not shown). Injection sites are located in POM nucleus, seen here as the large, bright eYFP spots medial to TRN. The smaller bands of eYFP along the medial and lateral edges of the somatosensory TRN are axons and terminals from the labeled POM cells. In addition to the TRN edges, POM also targeted L5a and L1 of barrel cortex (but not L4; data not shown). Top left image shows the injection site for Figure 2d.

b, Left, schematic showing recording configuration (also used in the experiments of Figure 2 c-f). Right, additional representative examples of synaptic responses of cells across the medial-lateral axis of somatosensory TRN evoked by POM stimulation. TRN cells near the edges of somatosensory TRN received strong input from POM whereas cells located in the center of TRN did not.

Extended Data Figure 8

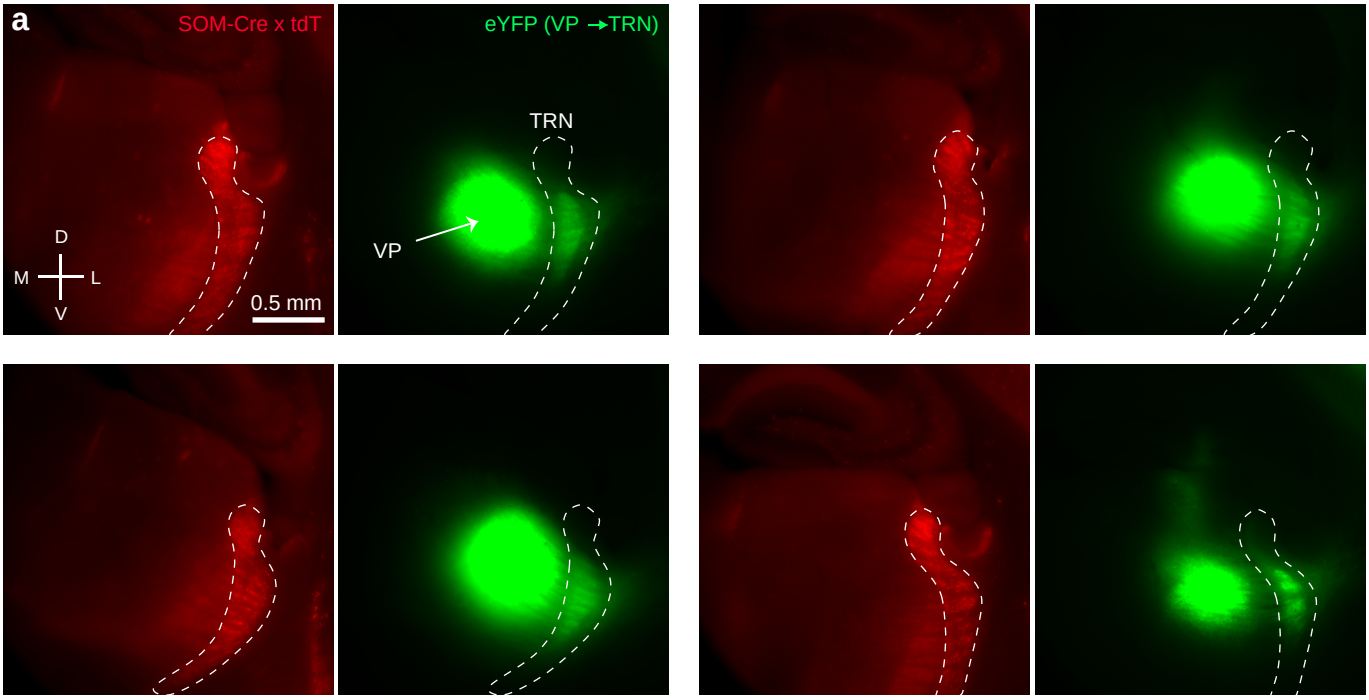

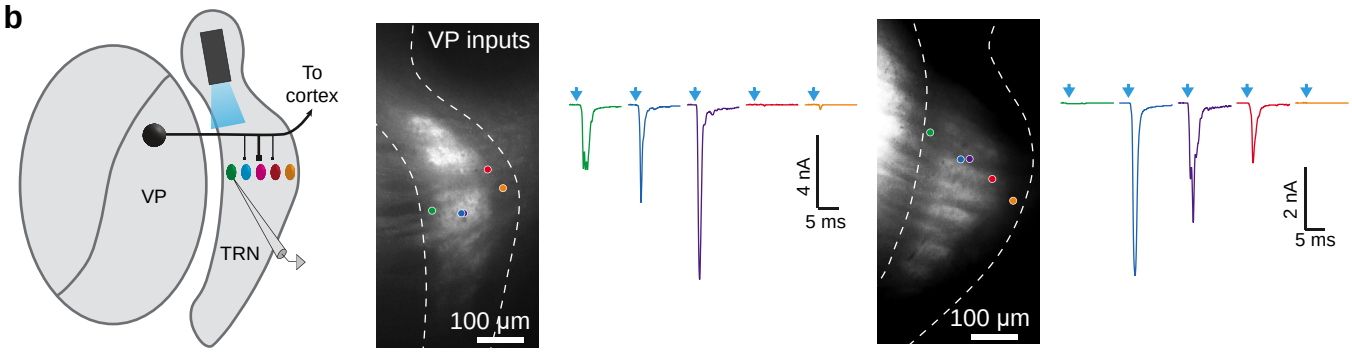

Extended Data Figure 8. VP afferents target the CB-dense center of somatosensory TRN. Similar to Extended Data Figure 7 except for VP rather than POM injections.

a, Representative examples showing the VP injection sites and anterograde projections to TRN in live 300 µm slices. VP afferents clearly targeted the central zone of TRN. VP also projected to L4 of barrel cortex but not L5a or L1 (not shown). Top left image shows the injection site for Figure 2i.

b, Left, schematic showing recording configuration (also used in the experiments of Figure 2 g-j). Right, additional representative examples of synaptic responses of cells across the medial-lateral axis of somatosensory TRN evoked by VP stimulation. Cells in the center of somatosensory TRN received strong input from VP whereas cells located near the edges of TRN did not.

Extended Data Figure 9

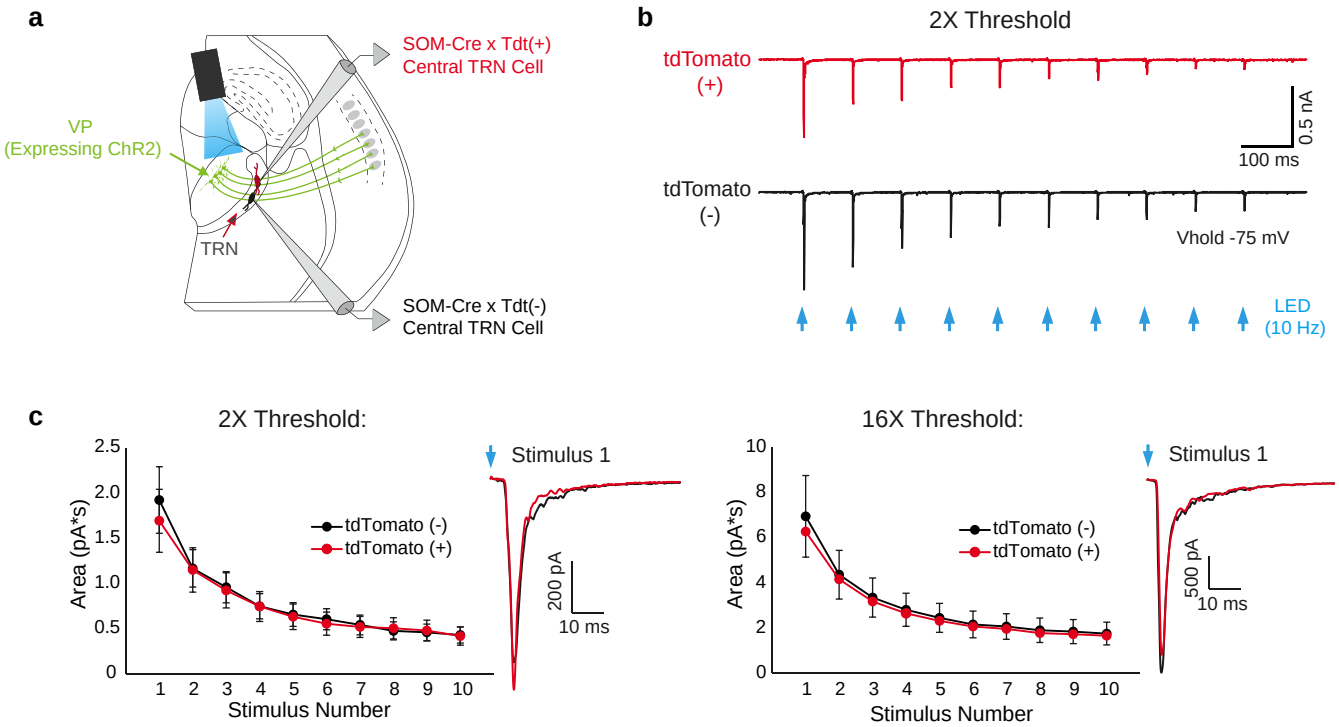

Extended Data Figure 9. SOM-Cre x tdTomato positive and negative neurons in the central zone of somatosensory TRN receive similar synaptic input from VP

a, Left, schematic showing experimental design. Recordings were made in 300 µm thick slices from SOM-Cre X Ai14 mice. ChR2-eYFP was virally expressed in VP cells. We optically stimulated the VP cells/axons and recorded evoked synaptic responses from closely spaced tdTomato (tdT) positive and tdT negative neurons in the central zone of TRN. We ensured that both cells had similar eYFP terminal labeling surrounding them - usually the cells were separated by less than 50 µm. The goal was to test if there were any response differences between central TRN cells that were SOM-Cre x tdT positive versus negative. Neurons were tdT positive if they expressed Cre recombinase at any stage of their lives; in central zone TRN of SOM-Cre mice, neurons appeared to express Cre only early in development (see main text; Fig. 1b, g; Extended Data Fig. 1a, 4, 5, 6).

b, Average optically-evoked synaptic responses (1-ms LED pulses, 10 Hz trains) for tdT positive and tdT-negative cells (stimulation at 2X threshold for a clear EPSC). Threshold intensity was not significantly different between tdT positive and tdT negative cells. The average LED power used at 2x threshold was 2.13mW.

c, Short-term EPSC depression (left) and kinetics (right) do not differ between tdT positive and negative cells at 2X Threshold (n=21 pairs of cells) or at 16X Threshold (n=12 pairs of cells) (ANOVA, $p=0.96$ and $p=0.61$, respectively; All $p>0.05$, Bonferroni's t- test). Thus, VP synaptic inputs appear to be no different for central TRN cells that expressed SOM-Cre during early development than for those that are SOM-Cre negative continuously.

Extended Data Figure 10

a Short-term synaptic depression: Similar effects for the initial and full responses

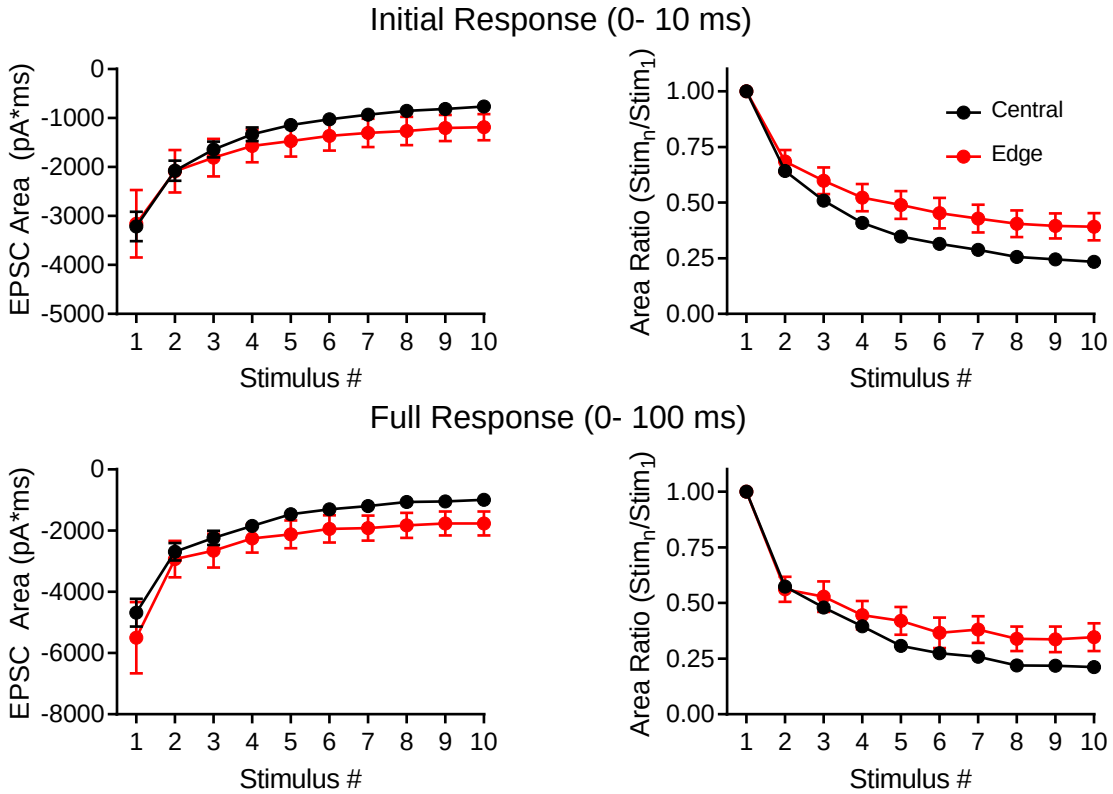

b Short-term synaptic depression: Similar effects for weak and strong responses

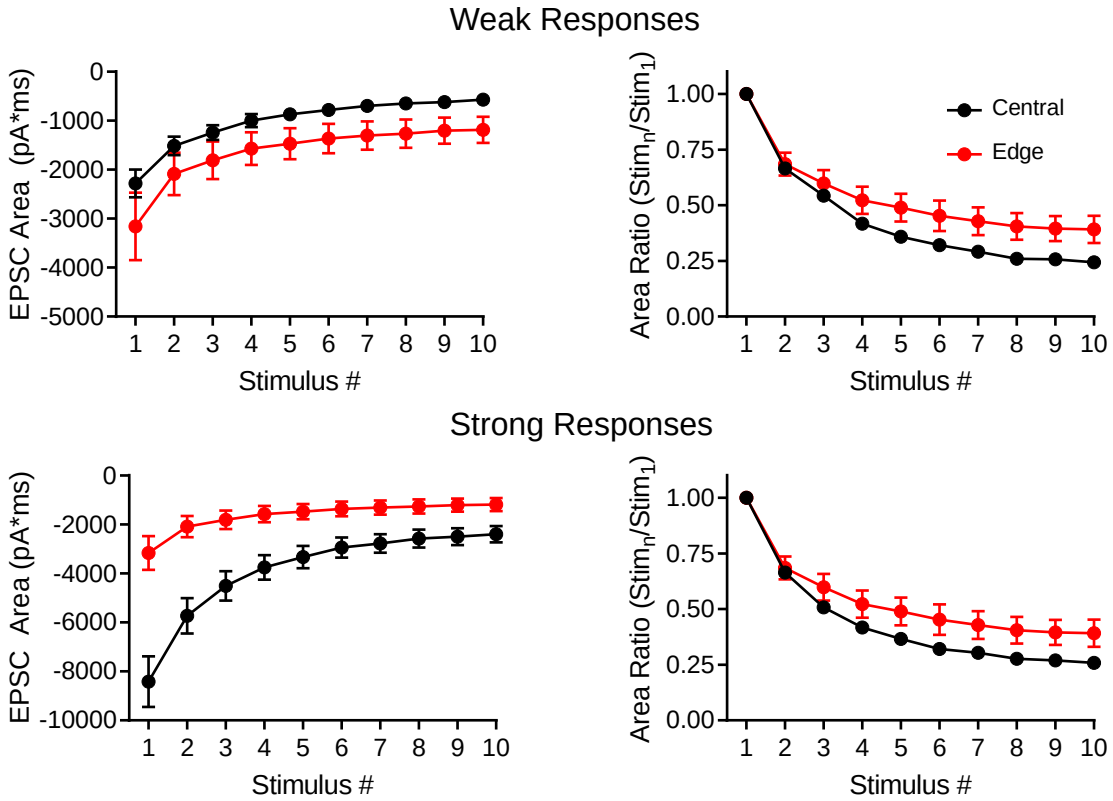

Extended Data Figure 10. Differences in short-term depression between edge and central cells are independent of stimulus strength and temporal components of the responses measured (i.e., early vs late response components).

a, Short-term synaptic depression is similar whether EPSCs are measured only during the initial fast components of the responses (the first 10 ms) or across longer durations (100 ms). ChR2-expressing VP and POM inputs were optically stimulated (1-ms LED pulse, 10 Hz stimulus) and EPSCs were recorded in central and edge cells, respectively.

Top row, raw EPSC areas (left) and normalized area dynamics (right) for the initial 10 ms of the responses (top right is the same plot shown on Fig. 3C). The response areas were similar for central and edge cells to stimulus 1 (unpaired t-test, two-tailed, P=0.93). There was greater short-term depression for the central cells than the edge cells ($p < 0.0001$, ANOVA stim. 2-10; All $p < 0.005$ from stimulus 5-10, Bonferroni's t- test).

Bottom row, raw EPSC areas (left) and normalized area dynamics (right) for the full response (0-100 ms). Again, there was greater short-term depression for the central cells than the edge cells ($p < 0.0001$, ANOVA stim. 2-10; $p < 0.05$ for stimulus 7 and 10, Bonferoni's t-test. Central cells: 42 cells from 10 mice. Edge cells: 14 cells from 7 mice.) Thus, the overall short-term synaptic depression patterns are similar for early and later components of the EPSCs.

b, Differences in short-term depression of central and edge cells does not change with varying input strength. Maximum response amplitudes tended to be larger for central than for edge cells. Here we compare short-term depression of synaptic responses in central and edge cells, varying stimulus intensities for the central cells to either roughly match the response amplitudes of edge cells (top row) or drive central cell responses significantly higher than those of edge cells (bottom row).

Left, raw EPSC areas. Responses of edge cells are equal in the top and bottom rows whereas responses of central cells are weaker in the top row and stronger in the bottom row.

Right, EPSC short term synaptic dynamics for the data from the left. There were no major differences in patterns of short-term synaptic depression for the weaker versus stronger responses. In both cases, there was more depression for the central cells than the edge cells ($p < 0.0001$, ANOVA stim. 2-10; All $p < 0.05$ from stimulus 5-10, Bonferoni's t-test). Central responses were acquired at 2X response threshold for the top row (LED Power: 1.92 mW, n= 49 cells from 11 mice) and 16X response threshold for the bottom row (LED Power: 11.9 mW, n= 32 cells from 11 mice).

Extended Data Figure 11

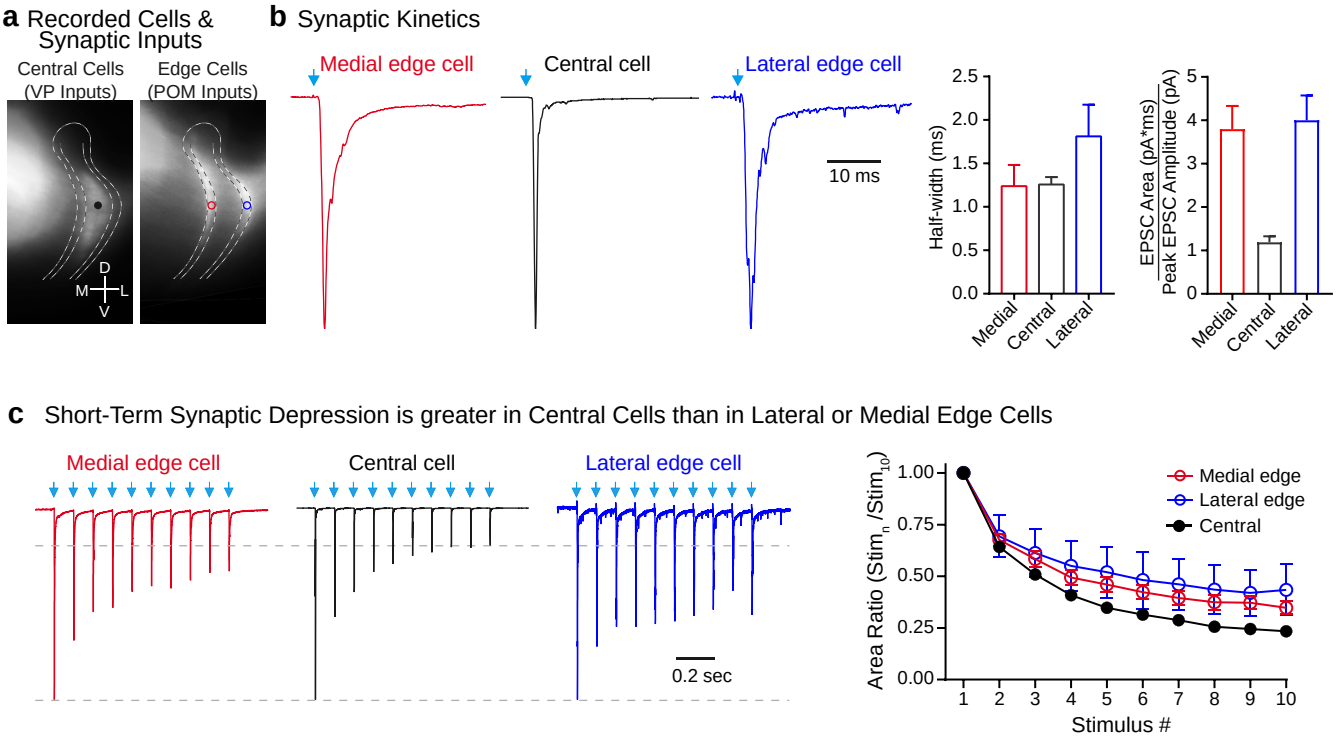

Extended Data Figure 11. Breakdown of EPSC kinetics and short-term synaptic depression based on topography.

a, Schematic showing approximate locations of TRN somas targeted for each subcircuit. EPSCs in medial and lateral edge cells were examined separately here, using the dataset from Figure 3 a-c. Vclamp at -84 mV.

b, Kinetics of the EPSCs. Left, optically evoked EPSCs for cells of each group (stimulus 1 of (c)). Right, Half-widths of EPSCs were not different between central and edge cells ($p=0.11$, ANOVA, All $p>0.05$ for Bonferroni's t- test). However, EPSCs evoked by POM inputs to medial and lateral edge cells were broader, with greater fractional areas in the later portions of the responses, than EPSCs evoked by VP inputs to central cells (quantified as the ratio of the area to the peak amplitude). This ratio varied as a function of cell group ($p<0.0001$, ANOVA). The two edge groups were not different from one another (posthoc, Bonferroni's t-test, $p>0.99$). Central responses were significantly different from medial and lateral edge responses (posthoc, Bonferroni's t-test, $p<0.0001$).

c, Left, representative traces showing the short-term synaptic dynamics of optically evoked EPSCs across groups (10-Hz trains of LED stimuli - arrows). Right, average EPSC areas measured during the first 10 ms of the responses. Short-term synaptic depression varied across groups. Depression in the two edge cell groups did not differ significantly (Bonferroni's t-test, $p=0.08$). Depression of VP evoked responses in central cells was stronger than depression of POM evoked responses in medial or lateral cells (Bonferroni's t-test; central vs. lateral and central vs. medial, $p<0.0001$; central group: 42 cells from 7 mice, medial and lateral groups: 7 cells each from 7 mice).

Extended Data Figure 12

a Optical stim within TRN: Over the terminals of the ChR2-expressing TC cells

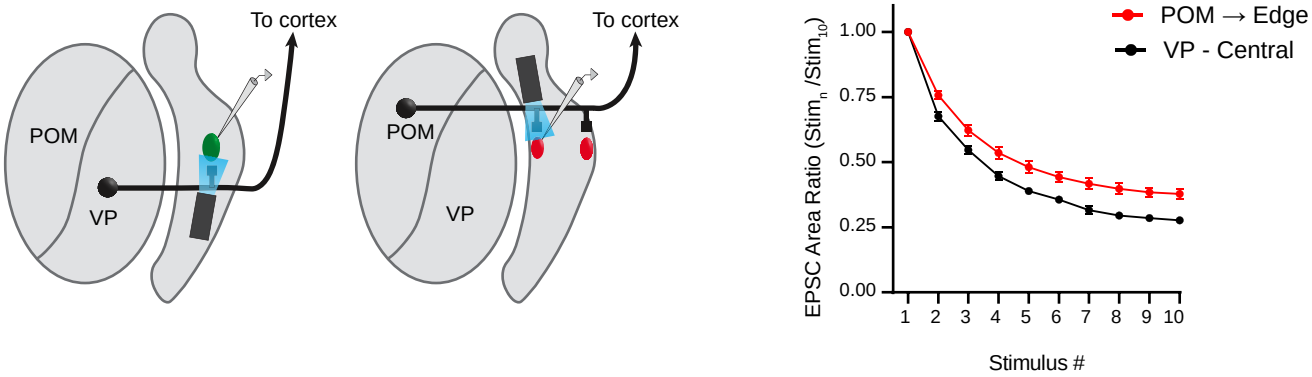

b Optical stim within TC nuclei: Over cell bodies and proximal axons of the ChR2-expressing TC cells

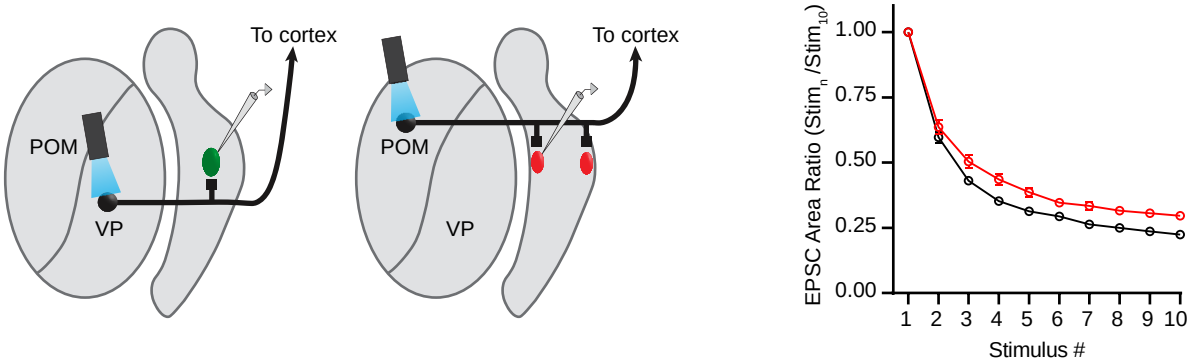

c Optical control stim: Away from the ChR2-expressing pathway to test influence of light scattering

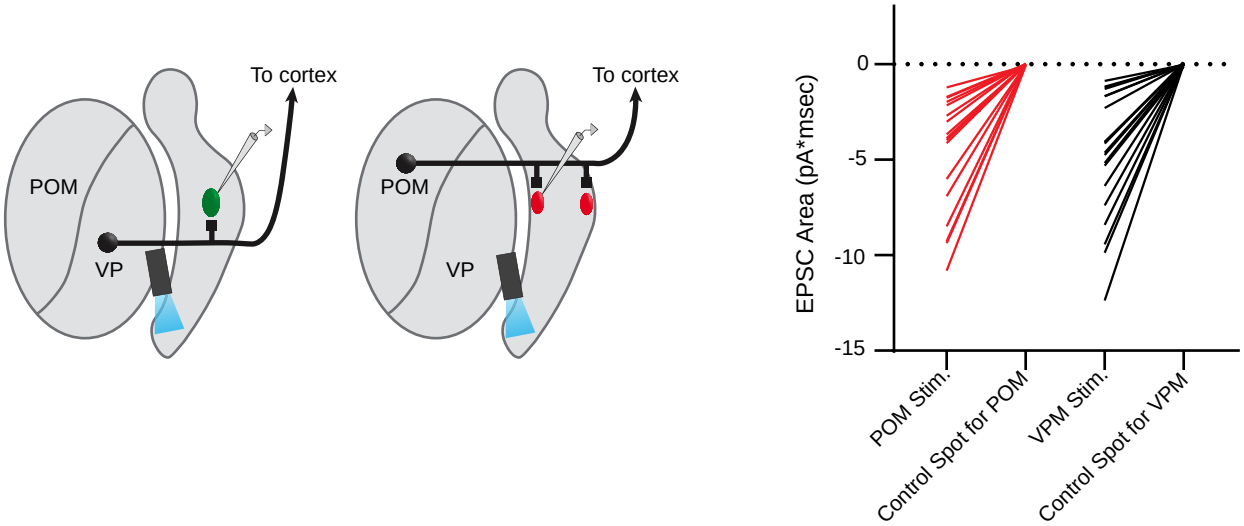

Extended Data Figure 12. Differences in short-term depression between the two somatosensory thalamoreticular pathways are similar when stimulating over the presynaptic ChR2-expressing cell bodies or over their terminals

Some studies have shown that release probability and short-term synaptic plasticity can can be abnormal when optogenetic light stimuli are directed at opsin-expressing presynaptic terminals (e.g., Jackman et al, *J. Neurosci.* 34(22):7704-14, 2014). We address this issue in the experiments described below.

a, VP synapses onto central TRN cells undergo greater short-term depression than POM synapses onto edge cells when optically stimulating the TC terminals within TRN. Left, Schematic showing recording configuration when optically stimulating over the terminals of the ChR2-expressing TC cells. For all experiments in this figure (a-c), $GABA_A$ receptor responses and T-type calcium channels were blocked by applying picrotoxin (50 µM) and TTA-P2 (1 µM), respectively. Right**,** average short-term synaptic depression. Light intensities were chosen to evoke ~ 1.5 - 3 nA peak responses. EPSC areas were measured over the first 10ms of each response. There was greater short-term depression for the VP→Central cell pathway (n=20 cells from 5 mice) than the POM→Edge cell pathway (n=17 cells from 8 mice) ($p < 0.005$, ANOVA stim. 2-10; All $p < 0.05$ from stimulus 5-10, Bonferroni's t-test).

b, VP inputs to central cells remain more depressing than POM inputs to edge cells when stimulating within the TC nuclei. Left, schematic showing recording configuration when optically stimulating over cell bodies and proximal axons of the ChR2-expressing TC cells. Right, Average short-term synaptic depression was greater in central than edge cells ($p < 0.005$, ANOVA stim. 2-10; All $p < 0.05$ from stimulus 5, 7-10, Bonferroni's t-test). This pattern of short-term depression in central cells (VP inputs) and edge cells (POM inputs) did not differ from the previously observed pattern in the same group of cells when stimulating over the TC terminals (panel a) or in previous experiments (Fig. 3, Extended Data Fig. 9-11).

c, Optical control indicating that light scattering/spread to the TC terminals did not trigger the responses observed when stimulating within TC nuclei (as in panel b). Left, Schematic showing recording configuration. The LED was directed to ventrally-located 'control spots', away from the ChR2-expressing TC pathway but equally distant from the TC terminals as the effective stimulus spots within the TC nuclei. Therefore, if synaptic responses were observed, they would be triggered by light spreading to the ChR2-expressing TC terminals within the TRN. Right, EPSC areas when stimulating over the TC nuclei vs. the control spots using matching LED intensities. No clear responses were evoked when stimulating over the control spots, suggesting that light

spread to the terminals did not drive the responses when stimulating within the TC nuclei ($p<0.0001$ ANOVA, Bonferoni's t-test).

Extended Data Figure 13

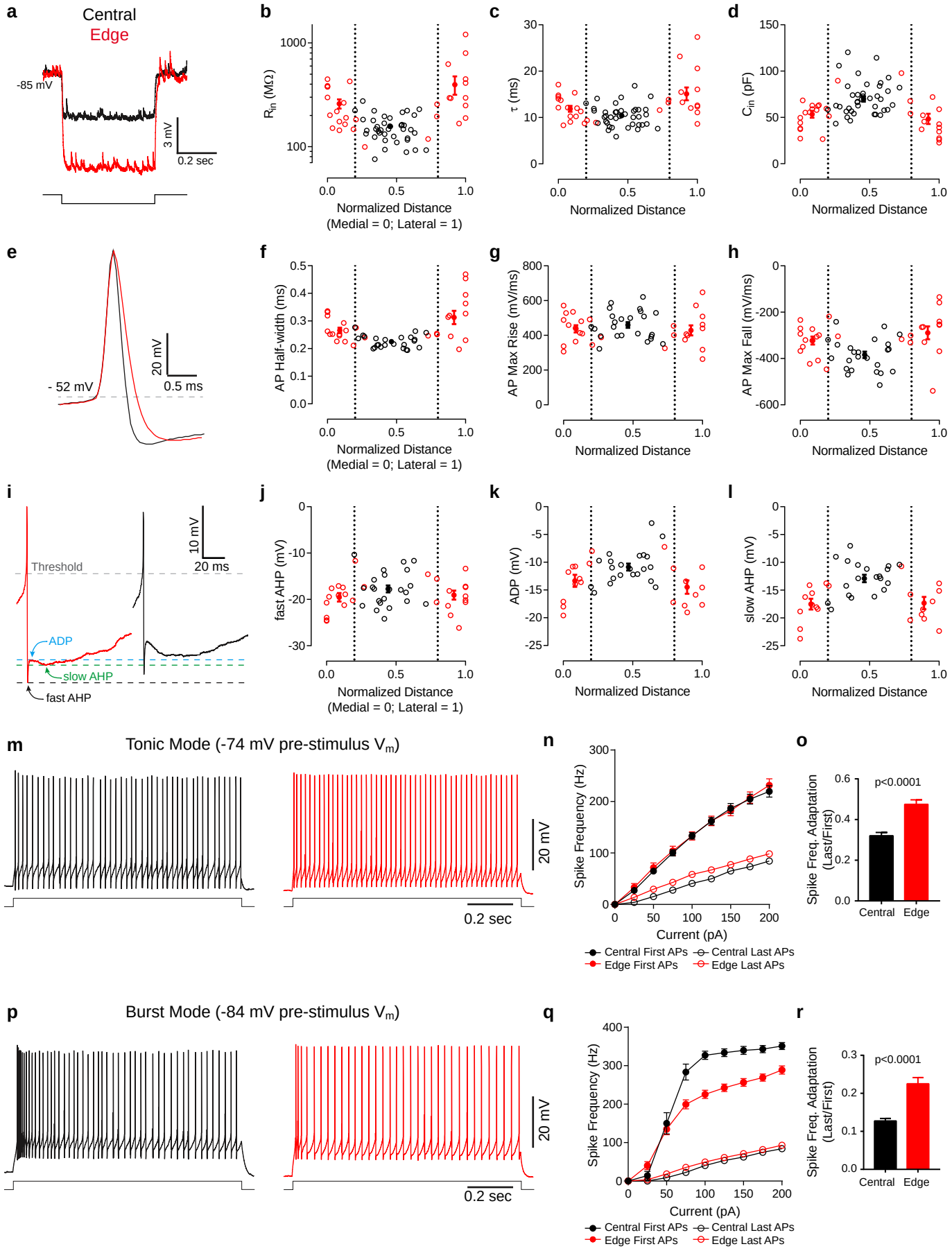

Extended Data Figure 13. Intrinsic physiological properties vary between central and edge cells, in a graded manner.

a, Voltage responses to hyperpolarizing current steps (-25 pA) for representative central and edge cells. Throughout this figure, central cells are colored black and edge cells are red. Note the higher input resistance for the edge cell (edge example = 316 MΩ; central example = 152 MΩ).

b-d, Group data. Input resistances (b), time constants (c), and membrane capacitances (d) for central (black) and edge (red) cells as a function of medial-lateral soma position (far medial edge = position 0, far lateral edge = position 1; steady-state V_m ~ -84 mV). Open circles show individual cell measurements. Filled circles show averages for the cell groups: medial edge cells, central cells, and lateral edge cells.

e, Representative examples of edge and central cell action potentials (APs).

f-h, AP properties as a function of soma location. Half-width (f), AP peak rising slope (g), AP peak repolarization slope (h). Edge cells have wider APs due to slower repolarization slopes, suggesting differences in potassium channels.

i, Representative AP afterpotentials of each cell type. Edge cells generally have a more hyperpolarized fast-afterhyperpolarizations (fast-AHPs), afterdepolarizations (ADPs), and slow-afterhyperpolarizations (slow-AHPs).

j-l, fast-AHP (j), ADP (k), and slow-AHP (l) for medial edge cells, central cells, lateral edge cells as a function of somatic location (APs evoked from a steady state V_m ~ -74 mV; values relative to spike threshold).

m, Representative examples of repetitive firing evoked by 75 pA current steps (from -74mV baseline potentials) for central and edge cells. When excited from -74mV, central and edge cells discharge APs in tonic mode.

n, Spike Frequency vs. Current Intensity (FI) plot for central and edge cells. Closed circles show the AP frequency for the first 2 APs in each spike train. Open circles show the AP frequency for the last 2APs. The initial AP frequency is similar between edge and central cells at multiple current steps. Yet, edge cells fire at higher frequencies than central cells by the end of the current pulses, likely because edge cells have higher input resistances.

o, Central cells have more spike frequency adaptation than edge cells. Spike frequency adaptation was measured as frequency of the last 2 APs/frequency of the first 2APs. Bar graphs show average adaptation ratio for responses to 175-200 pA currents (firing rates by the end of the trains ranged from 40-100 Hz).

p-r, Same as m-o except responses evoked from steady-state potentials of -84 mV. At -84mV, central and edge cells discharge APs in burst mode and central cells show more pronounced

bursts than edge cells. Traces from the same example cells are shown in panels m and p. On average, central cells had higher spike thresholds than edge cells when stimulated from -84 mV steady-state potentials (q) (see Extended Data Table 1 for more threshold information). But, the initial AP frequencies for central cells were much higher than edge cells due to their bursty nature (q). Yet, the AP frequencies by the end of the trains were not significantly different between central and edge cells (q). Central cells have stronger spike frequency adaptation than edge cells (r), largely due to stronger initial bursting in central cells. For measurements of adaptation ratios for spiking evoked from -84 mV, responses with end firing rates ranging from 20-60Hz were used. For panels a-r: central and edge cell recordings were interleaved within slices (drawn from at least 8 mice per measured property). See Extended Table 1 for additional intrinsic physiological properties.

Extended Data Figure 14

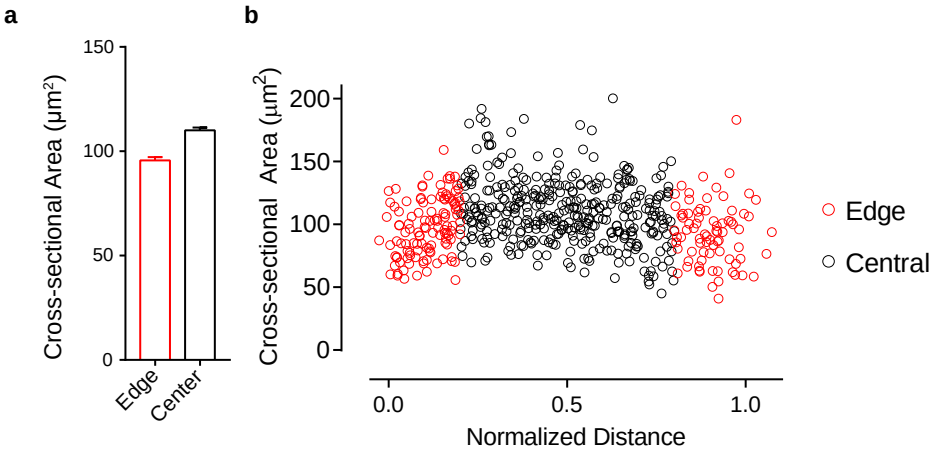

Extended Data Figure 14. Central cells have larger somata than edge cells

a, ROIs outlining neural somata were hand-drawn with the aid of ROIManager (ImageJ) using the PV-IHC tissue from Figure 1 (n=575 cells; 3 sections from 3 mice). Cells were included only if the somas were completely present in the 40-um sections. Central cells (black) have larger cross-sectional areas than edge cells (red). (Mean areas: central = 110.05 μm^2, edge = 95.59 μm^2; t-test, unpaired, two-tailed, $p<0.0001$).

b, Cell areas gradually change with location - the cells near the outer edges are smaller and areas increase toward the center of TRN.

Extended Data Figure 15

a Outputs from CB+ TRN Central Cells (example preparation)

Projections of Calb1-Cre TRN cells

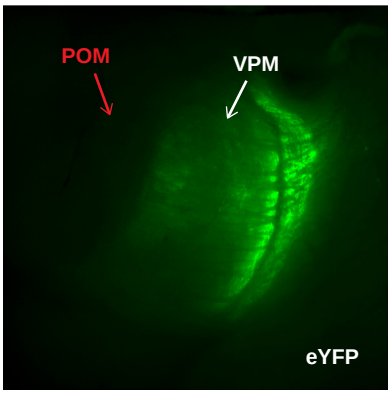

Synaptic recording sites in VPM & POM

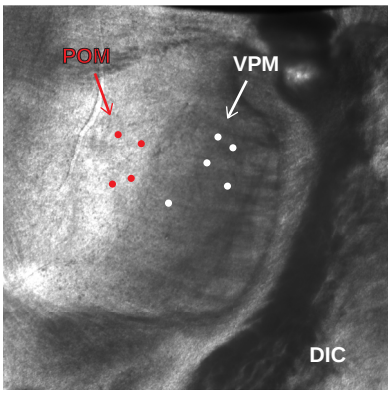

Stimulation of CB+ TRN Central Cells evoked strong IPSCs in VPM

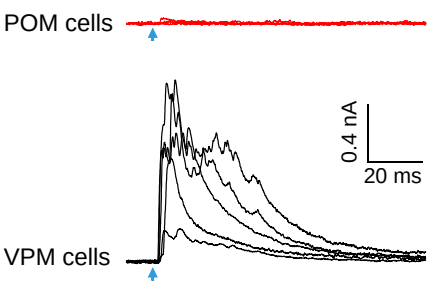

b Outputs from SOM+ TRN Edge Cells (example preparation)

Projections of SOM-Cre TRN cells

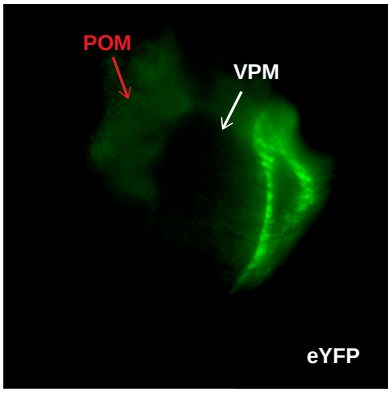

Synaptic recording sites in VPM & POM

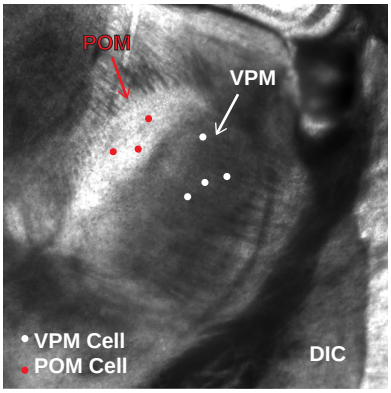

Stimulation of SOM+ TRN Edge Cells evoked strong IPSCs in POM

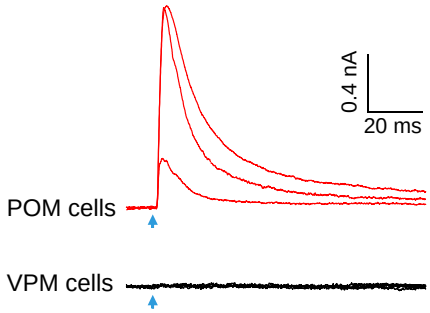

c Group Data

Normalized fluorescence of TRN axonal projections within the target thalamic nuclei

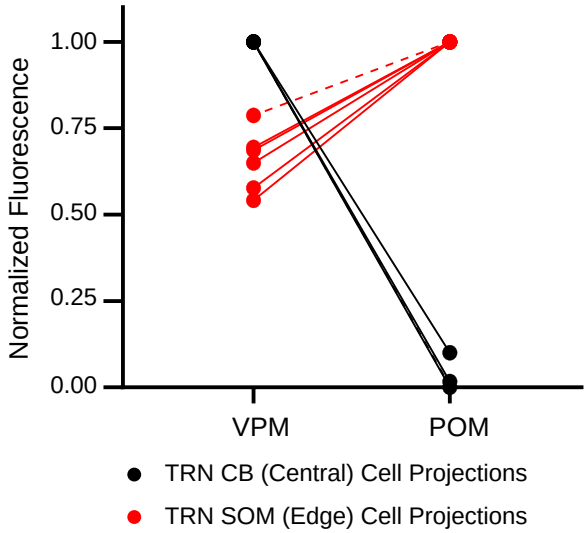

IPSC strengths

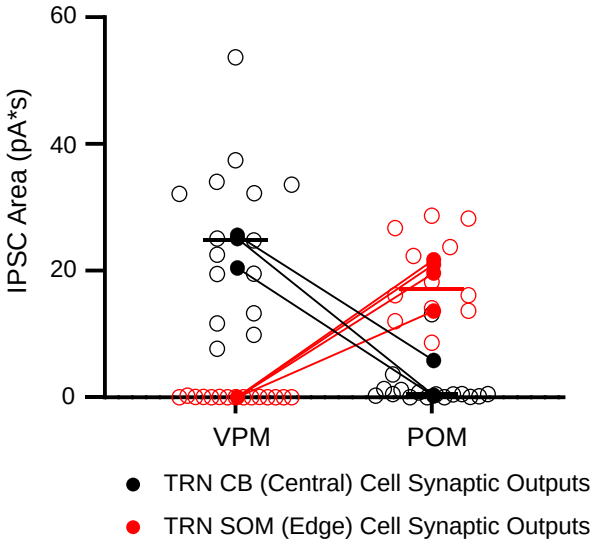

Extended Data Figure 15. Inhibitory output from TRN: CB-expressing TRN central cells project to VPM, whereas SOM-expressing TRN edge cells project to POM.

a, Fluorescence (left) and DIC (middle) images from a live 300 µm slice following ChR2-eYFP expression in Calb1-Cre positive (TRN central) cells. Fluorescent axons of these TRN central cells target VPM but not POM. White and red colored circles show the locations of recorded VPM and POM neurons, respectively. Right: Strong IPSCs were evoked in VPM (black) whereas virtually no IPSCs were evoked in POM (red) by optical activation of CB-Cre TRN central cells (Each trace is an average of 10 sweeps, V_m -6 mV). Arrows indicate onsets of LED flashes (1ms duration). Glutamate receptors were blocked by applying APV (50 µM) and DNQX (20 µM).

b, Same as (a) except ChR2-eYFP expression was in SOM-Cre TRN Edge cells. Notice the strong axonal targeting and IPSCs in POM rather than VPM.

c, left: Group plot comparing fluorescence projection intensities to VPM and POM from the two TRN cell types. Fluorescence was normalized to the maximum level across the thalamic relay nuclei, with zero values set to the minimum level in the slice (n=6 slices from 5 SOM-Cre mice and 4 slices from 3 Calb1-Cre mice; dashed lines represent a second slice for a mouse). Projections of CB+ TRN cells were stronger in VPM than in POM, whereas projections of SOM+ TRN cells were stronger in POM than in VPM (all $P<0.0001$, ANOVA).

c right: Strengths of IPSCs recorded in VPM and POM reflected their anatomical inputs from TRN. IPSCs evoked by optical stimulation of CB+ TRN central cells (black) were large in VPM (n=15) and very weak in POM (n=16). Conversely, IPSCs evoked by stimulation of SOM+ edge (red) cells were strong in POM (n=12 cells) and essentially undetectable in VPM (n=15 cells). Open circles show response areas for individual cells. Closed circles show averages per mouse. ($P<0.0001$, ANOVA). Comparisons were made using matched LED power.

Extended Data Figure 16

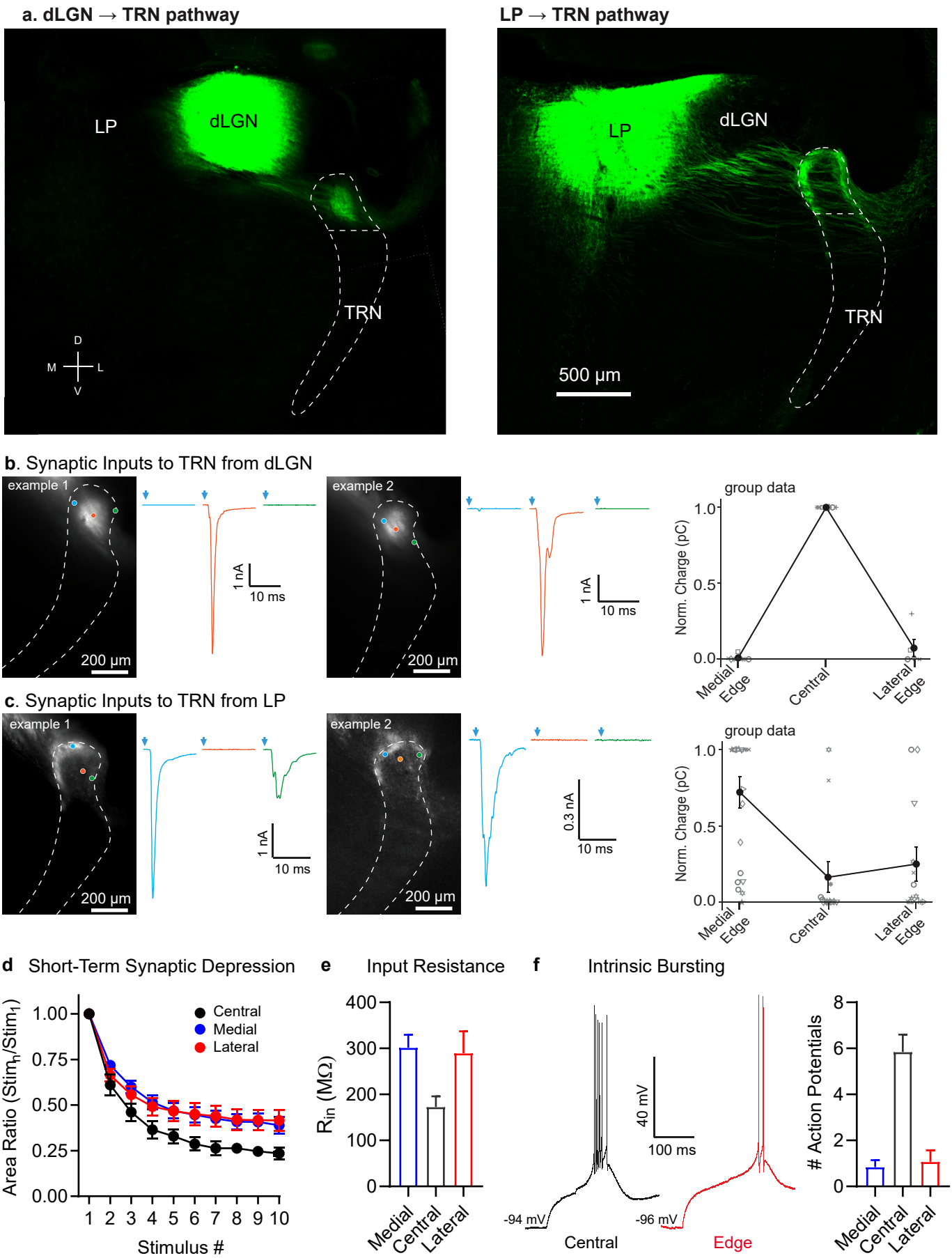

Extended Data Figure 16. In the visual TRN, the organization of thalamic inputs and physiological characteristics of the cells are comparable to the somatosensory system

a, Representative confocal images showing the dLGN (left) or LP (right) injection sites and anterograde projections to TRN. dLGN projects to the central zone of the visual sector of TRN whereas LP projects to the edges of the visual sector of TRN. The TRN was outlined using the tdTomato reporter expression or IHC for parvalbumin; approximate ventral boundaries of the visual sector indicated by horizontal dashed lines. Brains were sectioned in the TC plane to facilitate comparison with other experiments of the study.

b, Two representative examples (left and middle panels) of synaptic responses of cells across the medial-lateral axis of visual TRN evoked by optical dLGN stimulation. Cells in the center of visual TRN received strong input from dLGN whereas cells located near the edges of TRN did not (average of 10 sweeps, -84 mV). Right, Relationship between soma location in TRN and evoked synaptic response (n=19 cells from 6 preps, each prep represented by a different symbol shape) shows that cells in the center of visual TRN respond strongly to dLGN input and those in the medial and lateral edges have minimal dLGN inputs (as in Figure 2, and Extended Data Figs. 7-8).

c, Same as (b) except characterizing synaptic input to TRN from LP. Cells along the medial edge (and in some cases along the lateral edge) of visual TRN received strong input from LP. In contrast, cells located in the center of visual TRN generally had weak or no responses to LP input (average of 10 sweeps, -84 mV; n=49 cells from 12 preps).

d, Average short-term synaptic depression of visual thalamoreticular responses. Light intensities for were chosen to evoke ~2.5 nA peak responses (average LED powers: 20.8 mW for LP, 6.6 mW for dLGN). EPSC areas measured over the first 10ms of each response. There was greater short-term depression for the central cells than the edge cells ($p < 0.03$, ANOVA, stim. 2-10). Depression in the two edge cell groups did not differ (Bonferroni's t-test, all $p>0.99$). Depression of dLGN evoked responses in central cells was stronger than depression of LP evoked responses in medial or lateral cells (Bonferroni's t-test; central vs. medial, central vs. lateral, $p<0.0001$); central group: 7 cells from 5 mice, medial group: 17 cells from 12 mice, lateral group: 10 cells from 7 mice).

e, Group data comparing the input resistances of medial edge (n=16 cells from 14 mice), central (n=14 cells from 13 mice), and lateral edge cells (n=15 cells from 13 mice). Input resistance varied as a function of cell group ($p=0.02$, ANOVA). The two edge groups were not different from one another (posthoc, Bonferoni's t-test, $p=0.96$). Central cell input resistance was significantly

different from medial, although not from lateral (posthoc, Bonferoni's t-test, p=0.032, 0.062, respectively).

f, Central cells of visual TRN were more prone to bursting than those along the edges. Left, representative offset bursts. Cells were injected with negative intracellular current to produce a steady state V_m of ~95 mV, then the current was removed. Right, average number of action potentials during "offset bursts" (as in examples on left) was 5.8 ± 0.76 for central cells (n=19 cells from 15 mice), but only 0.8 ± 0.30 for medial cells (n=19 cells from 14 mice) and 1.1 ± 0.50 for lateral cells (n=14 cells from 12 mice) ($p<0.0001$, ANOVA). The two edge groups were not different from one another (posthoc, Bonferoni's t-test, p=0.96). The edge cells discharged far fewer action potentials per burst than the central cells (posthoc, Bonferoni's t-test, $p<0.0001$ for medial vs. central cells and lateral vs. central cells). Data shown as Mean ± SEM.

Extended Data Figure 17

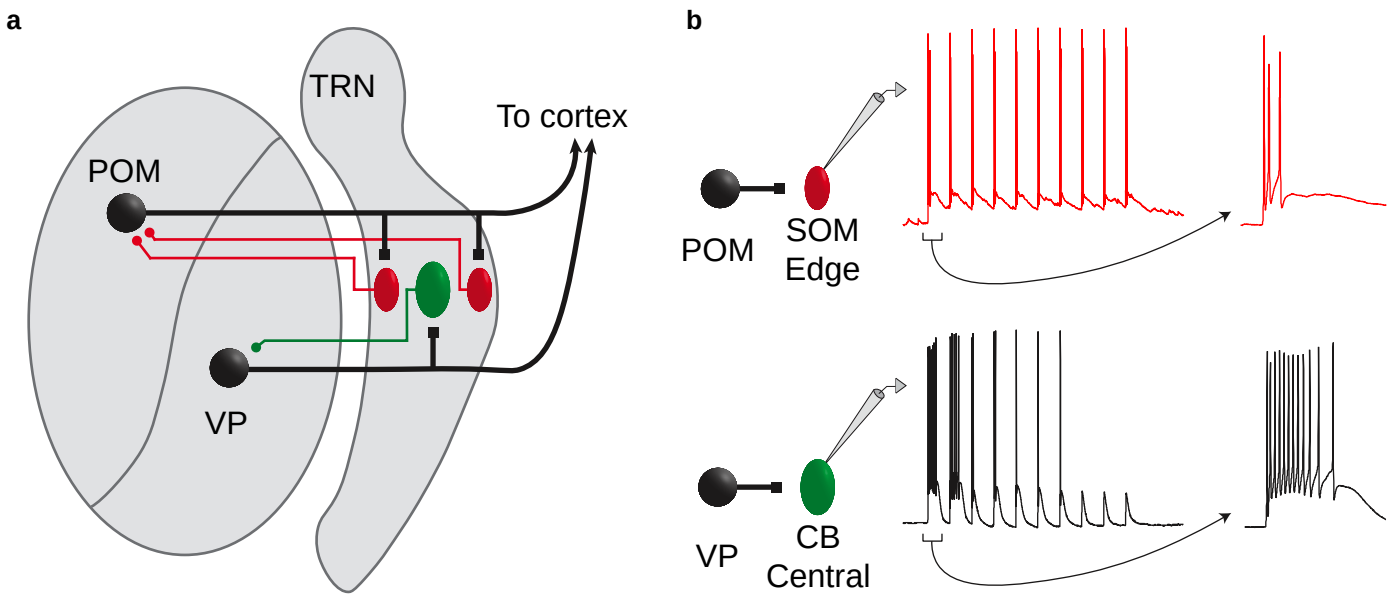

Extended Data Figure 17. Operational and organizational scheme for somatosensory circuits in the TRN.

a, Schematic illustrating the organization of the somatosensory sector of TRN. Inputs from the primary VP thalamic nucleus innervate the calbindin-dense central zone of TRN (green cells), whereas higher-order POM inputs innervate the somatostatin-dense edges (red cells). The inhibitory projections of the TRN cells to VP and POM appear to reciprocate their inputs (colored axons in the schematic). The spatial organization of the neurochemically distinct TRN cell types, and the stark segregation of their primary and higher order connections, suggests a core-shell organization for somatosensory circuits of the TRN.

b, Distinct responses of central and edge TRN cells to their thalamic inputs. The spike responses of central and edge cells are determined by the dynamic synaptic properties of their respective thalamic inputs and intrinsic physiological properties of the TRN cells themselves. The spiking of central cells evoked by VP input is phasic, with strong initial bursts that deeply depress with repetitive stimulation - consistent with a core circuit that processes transient sensory signals. In contrast, the spike responses of edge cells to POM input is more sustained, with initially weaker but more persistent activation – suited to processing temporally distributed higher-order signals. TRN: thalamic reticular nucleus; POM: posterior medial nucleus; VP: ventral posterior nucleus

Extended Data Table 1

Intrinsic physiological properties of central and edge TRN neurons

Somatosensory TRN						
	Burst Mode (-84 mV pre-stimulus V_m)			Tonic Mode (-74 mV pre-stimulus V_m)		
	Central Cells	Edge Cells	P values	Central Cells	Edge Cells	P values
Resting Potential (mV)	-83 ± 0.3 *(157)*	-85 ± 0.4 *(101)*	<0.0001	n/a	n/a	n/a
Input Resistance (MΩ)	157 ± 7.1 *(42)*	316 ± 40.5 *(31)*	< 0.0001	278 ± 24.3 *(33)*	495 ± 59.5 *(32)*	<0.001
Membrane Time Constant (ms)	10.4 ± 0.34 *(42)*	13.3 ± 0.76 *(31)*	<0.0005	17.5 ± 1.16 *(33)*	20.5 ± 1.22 *(32)*	0.08
Input Capacitance (pF)	70 ± 2.8 *(42)*	51 ± 3.2 *(31)*	< 0.0001	67 ± 2.6 *(33)*	49 ± 2.8 *(32)*	< 0.0001
Rheobase (pA)	61 ± 4.5 *(25)*	39 ± 4.1 (28)	<0.0005	24 ± 3.3 *(26)*	16 ± 2.4 *(28)*	<0.05
AP Threshold (mV)	-58 ± 0.7 *(25)*	-56 ± 0.8 (28)	<0.05	-56 ± 0.7 *(26)*	-55 ± 0.7 *(28)*	0.4
AP Amplitude (mV)	69 ± 1.6 *(22)*	72 ± 1.7 *(23)*	0.2	68 ± 1.5 *(24)*	69 ± 1.8 *(28)*	0.4
AP Maximum rate of rise (mV/ms)	488 ± 17.8 *(22)*	481 ± 18.6 *(23)*	0.8	459 ± 16.4 *(24)*	434 ± 17.1 *(28)*	0.3
AP Maximum rate of fall (mV/ms)	-400 ± 17.4 *(22)*	-336 ± 15.4 *(23)*	<0.01	-384 ± 14.1 *(24)*	-307 ± 15.8 *(28)*	<0.0005
AP Half-width (ms)	0.22 ± 0.005 *(22)*	0.27 ± 0.010 *(23)*	<0.0005	0.23 ± 0.005 *(24)*	0.29 ± 0.013 *(28)*	<0.0001
Fast Afterhyperpolarization (fast AHP) (mV)	-14.5 ± 0.71 *(22)*	-16.1± 0.82 *(22)*	0.2	-17.7 ± 0.78 *(23)*	-19.5 ± 0.72 *(23)*	0.09
Afterdepolarization (ADP) (mV)	*na*	*na*	*na*	-10.8 ± 0.64 *(22)*	-13.9 ± 0.80 (21)	<0.005
slow Afterhyperpolarization (slow AHP) (mV)	-18.2 ± 0.64 *(22)*	-20.1 ± 0.82 *(22)*	0.08	-12.9 ± 0.67 *(20)*	-17.4 ± 0.72 *(21)*	<0.0001
Offset Burst # APs	9.6 ± 0.85 *(34)*	2.3 ± 0.51 *(38)*	<0.0001	*na*	*na*	*na*
Offset Burst Peak Frequency (Hz)	364 ± 23.8 *(34)*	108 ± 23.2 *(38)*	<0.0001	*na*	*na*	*na*
Offset Burst Mean Frequency (Hz)	243 ± 15.4 *(34)*	87 ± 18.6 *(38)*	<0.0001	*na*	*na*	*na*
Spike Frequency Adaptation (Last/First)	0.13 ± 0.01 *(31)*	0.23 ± 0.02 *(42)*	<0.0001	0.32 ± 0.02 *(29)*	0.47 ± 0.02 *(40)*	<0.0001

Intrinsic physiological properties of central and edge TRN neurons

Visual TRN						
	Burst Mode (-84 mV pre-stimulus V_m)			Tonic Mode (-74 mV pre-stimulus V_m)		
	Central Cells	Edge Cells	P value	Central Cells	Edge Cells	P value
Resting Potential (mV)	-84 ± 0.3 *(21)*	-85 ± 0.4 *(42)*	0.47	*na*	*na*	*na*
Input Resistance (MΩ)	173 ± 23.3 *(14)*	296 ± 26.8 *(31)*	< 0.01	*na*	*na*	*na*
Membrane Time Constant (ms)	10.9 ± 0.75 *(14)*	12.4 ± 0.53 *(31)*	0.12	*na*	*na*	*na*
Input Capacitance (pF)	70 ± 4.3 *(14)*	51 ± 5.7 *(31)*	< 0.05	*na*	*na*	*na*
Offset Burst # APs	5.8 ± 0.76 *(19)*	0.9 ± 0.27 *(33)*	<0.0001	*na*	*na*	*na*
Offset Burst Peak Frequency (Hz)	207 ± 23.1 *(19)*	32 ± 11.3 *(33)*	<0.0001	*na*	*na*	*na*
Offset Burst Mean Frequency (Hz)	107 ± 8.0 *(19)*	25 ± 13.7 *(33)*	<0.0001	*na*	*na*	*na*

Extended Data Table 1. Intrinsic physiological properties of central and edge TRN cells. Passive membrane properties, action potential (AP) dynamics, and repetitive firing properties for central and edge cells are shown for somatosensory TRN (page 1) and visual TRN (page 2). Properties were measured in current clamp mode, with steady-state V_m set to either -84 mV ("burst mode", left) or -74 mV ("tonic mode", right). "Offset bursts" are intrinsic bursts triggered by the offset of hyperpolarizing injected current, as illustrated in Fig. 3d and Extended Fig. 16f. The numbers of cells are shown in parenthesis. T-tests were unpaired, two-tailed. Data are shown as mean ± SEM.

Methods

Animals: All procedures were approved by the Brown University Institutional Animal Care and Use Committee. The following mouse lines were used: SOM-IRES-Cre (The Jackson Laboratory, 013044), PV-Cre (The Jackson Laboratory, 008069), Calb1-IRES-Cre-D (The Jackson Laboratory, 028532), Vgut2-IRES-Cre (The Jackson Laboratory, 016963), GPR26-Cre (STOCK Tg(Gpr26-cre)KO250Gsat/Mmucd, MMRRC), Ai14 (The Jackson Laboratory, 007908), ICR (Charles River, CD-1[ICR], Strain Code 022). To fluorescently target Somatostatin (SOM) or Parvalbumin (PV) cells in TRN, we bred the respective homozygous Cre mice (SOM-IRES-Cre, PV-Cre) with homozygous Cre-dependent tdTomato reporter mice (Ai14). In some experiments we instead injected viruses carrying Cre-dependent GFP genes into Cre mice (specified in the descriptions of the individual experiments, below). Of the 124 mice used in this study, 91 had C57 genetic backgrounds, 10 had ICR genetic backgrounds, and 23 had mixed C57/ICR backgrounds. Mice were maintained on a 12:12-hr light-dark cycle, group-housed, and provided food and water ad libitum.

Immunohistochemistry: Mice from postnatal ages 22-26 days were deeply anesthetized with Beuthanasia-D and intracardially perfused with 0.1M phosphate buffer (PB) followed by 4% paraformaldehyde (in PB). Brains were post-fixed overnight at 4℃ in the same fixative and then transferred to a 30% sucrose/0.1M PB solution until sectioning (4℃, 2-3 days). Forty µm-thick brain sections were cut on a freezing microtome at a somatosensory thalamocortical plane (35 degree tilt from coronal)* designed to contain the somatosensory thalamus, TRN, barrel cortex and many of their interconnections. Next the sections were immunostained. Briefly, they were washed 5 times in 0.1M phosphate buffer containing 0.15M NaCl, pH 7.4 (PBS) (5 min per wash), pre-incubated for 2 h at room temperature with a blocking solution (10% normal goat serum, 2% Triton X-100, 0.1% Tween 20 in 0.1M PB), then incubated with primary antibodies for 5 days at 4℃. After the primary incubation, sections were washed 8 times in PBS (5 min per wash), pre-incubated for 2 h in blocking solution, incubated with a secondary antibody solution for 3 days at 4℃, then washed 8 times in PBS and 3 times in PB (5 min per wash). Sections were mounted and cover-slipped using Prolong Gold or Prolong Gold with DAPI (Molecular Probes P36930 or P36931). Primary antibodies were: mouse monoclonal anti-parvalbumin (1:1000, Swant clone 235), rabbit polyclonal anti-Calbindin D-28k (1:1000 Swant clone CB-38a), mouse monoclonal anti-Calbindin D-28k (1:1000 Swant clone 300), rabbit polyclonal anti-Somatostatin-14 (1:1000; Bachem T4103), mouse monoclonal anti-NeuN (1:1000, Millipore MAB377). Secondary

antibodies were goat anti-mouse IgG (H+L) Cross-Adsorbed Secondary Antibody Pacific Blue (1:250, Molecular Probes P31582), goat anti-rabbit IgG (H+L) cross-adsorbed secondary antibody Alexa Fluor 647 (1:500, Molecular Probes A21244), goat anti-mouse IgG (H+L) cross-adsorbed secondary antibody Alexa Fluor 488 (1:250, Molecular Probes A11001), goat anti-rabbit IgG (H+L) highly cross-adsorbed secondary antibody Alexa Fluor 488 (1:250, Molecular Probes A11034). To test the specificity of the antibodies, no-primary and no-secondary controls were conducted for each. In addition, for the Calbindin antibodies, we performed assays in which the antibodies were pre-adsorbed with rat Calbindin D-28K protein (3.33 µg/1 µl of antibody, Swant recombinant rat Calbindin D-28) before tissue incubation. Confocal image stacks were taken on a Zeiss LSM 800, 20X objective, 0.26 µm pixel diameter.

For analysis of the immunohistochemical material, we selected sections spanning the somatosensory sector of TRN and the VP (approximately -1.7 mm to -1.1 mm from Bregma), generally focusing on the anterior-posterior center of that range (i.e., -1.4 mm from Bregma). The CellCounter ImageJ plugin was used to count cells positive for the tested markers. For accurate alignment across subjects and sections, small differences in TRN shapes were minimized by warping them to an average reference TRN image using the bUnwarpJ plugin in ImageJ. At least 12 landmark points were applied around the outer boundaries of each TRN (evenly spaced, 100 µm between points) for alignment. The TRN boundaries were identified using either the SOM-Cre x tdTomato or PV-Cre x tdTomato channel. Resulting corrections were applied to all channels.

<u>Fluorescence in situ hybridization (FISH)</u>: Mice (P21-P27) were deeply anesthetized with isofluorane and decapitated. The brains were removed while submerged in 4°C saline solution and fresh-frozen on liquid nitrogen. Frozen brains were sectioned (18 µm thick) at the somatosensory thalamocortical plane (described above) using a cryostat (Leica), adhered to SuperFrost Plus slides (VWR, 48311-703), and refrozen (-80°C) until used. Samples were fixed (4% PFA), processed as instructed in the ACD RNAScope Multiplex Fluorescent v2 Assay, and then immediately incubated with DAPI and cover-slipped with ProLong Gold (Molecular Probes P36930). Probes for PV (Mm-Pvalb-C3, Cat# 421931-C3), SOM (Mm-Sst, Cat# 404631), CB (Mm-Calb1-C2 Cat# 428431-C2), and tdTomato (tdTomato-C3 cat# 317041-C3) were purchased from Advanced Cell Diagnostics. Probes were visualized using the TSA® Plus Fluorescein (1:1000, Perkin Elmer NEL741E001KT), TSA® Plus Cyanine 3 (1:1000, Perkin Elmer NEL744E001KT), and TSA® Plus Cyanine 5 (1:1000, Perkin Elmer NEL745E001KT) evaluation

kits. Confocal image stacks were taken on a Zeiss LSM 800, 20X objective, 0.26 µm pixel diameter.

One section was selected from each of 6 mice for the FISH analysis. These sections were centered on the somatosensory sector of the TRN (approximately 1.4 mm posterior to Bregma). Four of the 6 mice were C57 wild-types. The remaining 2 mice were PV-Cre x Ai14 mice that expressed tdTomato in PV-Cre cells (the tdTomato-C3 probe, cat# 317041-C3, was used as a proxy for PV for these 2 mice). Images were quantified using ImageJ. Cell regions-of-interest (ROIs) were manually drawn for each cell based on the fluorescence signal of all three channels (SOM, CB, and either PV or tdTomato). For quantification, the mean fluorescence intensity for a cell's ROI was expressed as a percentage of the intensity range across the TRN of the section: (100 * mean Intensity for the cell's ROI) / (Maximum Pixel Intensity in the TRN - Minimum Pixel Intensity in the TRN). Cells were considered positive for an RNA marker if this normalized expression for the marker was greater than 7.5%, which best matched qualitative visual assessment of expression thresholds.

Probes for PV (Mm-Pvalb-C4, Cat# 421931-C4), Cre (CRE-C3, Cat# 312281-C3), and SOM (Mm-Sst, Cat# 404631) were used to assess correspondence between Cre and SOM mRNA expression in the SOM-Cre mouse line (4 SOM-Cre x ICR Mice).

Stereotactic Injection Procedure:

Mice were anaesthetized with a Ketaset-Dexdormitor mixture diluted in sterile saline (Ketaset, 70 mg/kg; Dexdormitor, 0.25 mg/kg; intraperitoneally). Once deeply anesthetized, mice were placed into a stereotactic frame, and a craniotomy was made over VP, POM, dLGN, LP, or TRN. Virus solution was then pressure-ejected into the brain via a glass micropipette attached to a Picospritzer pressure system at a maximum rate of ~ 0.05 µl/min (10-30 min total injection times). Following injection, the pipette was left in place for ~10 min before being slowly withdrawn from the brain. After surgery, mice were given Antisedan (2.5 mg/kg) to reverse the effects of Dexdormitor, and they were allowed to recover on a heating pad for ~1 h before being returned to their home cage. Experiments were usually performed ~ 10 d after the virus injections to allow for sufficient EGFP or opsin expression (mean: 10.4 ± 0.3, range: 8-19).

The following Adeno Associated Viruses (AAVs) and Lentiviruses were acquired from the University of North Carolina, Addgene or the University of Pennsylvania Vector Cores: (1) rAAV2/hSyn-ChR2(H134R)-eYFP-WPREpA (titer = ~3.93 x 10^{12} [vg]/ml), (2) pLenti-Synapsin-

hChR2(H134R)-EYFP-WPRE (titer = ~2.53 x 10^{10} [vg]/ml), (3) AAV2.Syn.DIO.hChR2(H134R)-EYFP.WP.hGH (titer = ~2.32 x 10^{13} [vg]/ml), (4) rAAV2/hSyn-ChR2(H134R)-mCherry-WPREpA (titer = ~2.2 x 10^{12} [vg]/ml), (5) AAV9.Syn.DIO.EGFP.WPRE.hGH (titer = ~6.25 x 10^{12} [vg]/ml), (6) rAAV2/Syn-Flex-ChrimsonR-TdT (titer = ~3.8 x 10^{12} [vg]/ml).

For experiments testing projections from specific thalamocortical nuclei to TRN (or from subtypes of TRN cells to thalamocortical nuclei) relatively small volumes (0.16 – 0.33 µl) of either AAV2 or lentivirus (described above) were stereotactically injected into individual presynaptic nuclei using the following mouse strains and coordinates. To test VP projections to TRN (Figs. 2-3, Extended Data Fig. 7, 9-12), virus was injected into SOM-Cre x Ai14 (n=15), ICR (n=4), Vglut2-Cre x ICR (n=5), or PV-Cre x Ai14 (n=1) mice between P12-16 (mean = P13.1 ± 0.2 d). Average coordinates from Bregma for VP were 1.99 mm lateral, -0.74 mm posterior, 3.08 mm depth. For POM projections to TRN (Figs. 2-3, Extended Data Fig. 8-12), virus was injected into SOM-Cre x Ai14 (n=8), ICR (n=6), PV-Cre x Ai14 (n=2), or GPR26-Cre x ICR (n=2) mice between P11-P14 (mean = P12.0 ± 0.3). Coordinates for POM were 1.36 mm lateral, -1.17 mm posterior, 2.86 depth. For dLGN projections to TRN (Extended Data Fig. 16), virus was injected into SOM-Cre x Ai14 (n=2), PV-Cre x Ai14 (n=2) or GPR26-Cre x ICR (n=1) mice between P14-19 (mean = P16.0 ± 0.8). Coordinates for dLGN were 2.38 mm lateral, -1.45 mm posterior, 2.35 depth). For LP projections to TRN (Extended Data Fig. 16), virus was injected into SOM-Cre x Ai14 (n=6), PV-Cre x Ai14 (n=6) or Calb-Cre x Ai14 (n=1) mice between P14-17 (mean = P15 ± 0.3). Coordinates for LP were 1.63 mm lateral, -1.36 mm posterior, 2.3 mm depth. For tests of the inhibitory outputs of TRN cell subtypes to VP and POM neurons, virus was injected into SOM-Cre x ICR (n=5), Calb-Cre x Ai14 (n=1) or Calb-Cre x ICR (n=2) mice between P12-15 (mean = 13.7 ± 0.3). Coordinates for these TRN injections were 2.2 mm lateral; -0.53 mm posterior, 3.0 mm depth.

For assessments of the positions of TRN cell subtypes (Fig. 1g, Extended Data Fig. 1, 5-6), relatively large volumes (1.3-2 µl) of AAV9 (described above) were injected across the entire dorsal-ventral extent of the TRN in SOM-Cre x Ai14 (n=10), SOM-Cre x ICR (n=2) or PV-Cre x Ai14 (n=4), or ICR (n=2) mice between P14 and P25 (mean 16.3 ± 0.9). Average coordinates for these TRN injections were 2.2 mm lateral; -0.53 mm posterior, with continuous outflow of virus solution from 2.2 to 4.4 mm depth.

<u>Slice Preparation:</u> Brain slices were prepared from P22-33 mice of either sex as previously described[40]. Mice were deeply anesthetized with isofluorane and decapitated. The brains were removed while submerged in cold (4°C) oxygenated slicing solution containing (in mM): 3.0 KCl,

1.25 NaH_2PO_4, 10.0 $MgSO_4$, 0.5 $CaCl_2$, 26.0 $NaHCO_3$, 10.0 glucose, and 234.0 sucrose. Brains were then mounted, using a cyanoacrylate adhesive, onto the stage of a vibrating tissue slicer (Leica VT1000 or VT1200S) and somatosensory thalamocortical brain slices (300 µm thick, 35 degree tilt from coronal[1]) containing VP, POM, TRN, S1, and portions of dLGN and LP were obtained. Slices were incubated for ~1 min in the cold sucrose-based slicing solution, then transferred for 20 min to a holding chamber containing warm (32°C) oxygenated (5% CO_2, 95% O_2) artificial cerebrospinal fluid (ACSF) solution. Finally, the slices were allowed to equilibrate in ACSF for 60 min at room temperature before imaging or recording. The ACSF solution contained (in mM): 126.0 NaCl, 3.0 KCl, 1.25 NaH_2PO_4, 1.0 $MgSO_4$, 1.2 $CaCl_2$, 26.0 $NaHCO_3$, and 10.0 glucose.

Live Imaging: 300 µm live sections centered on the somatosensory sector of TRN (-1.4 mm from Bregma) were imaged using Nikon or Zeiss upright microscopes with 2.5-5X objectives and Andor Zyla sCMOS cameras. Both epifluorescent and transmitted light (brightfield) images were obtained to characterize the topographical positions of the TRN cell types and the connections between TRN and VP, POM, dLGN, and LP.

Whole-Cell Recording Procedure: Brain slices (300 µm) were placed in a submersion-type recording chamber maintained at 32 ± 1 ℃ and continuously superfused with oxygenated ACSF (above). Neurons were visualized for recording using DIC-IR optics with 40X water immersion objectives. Patch pipettes had tip resistances of 3-6 MΩ when filled with a potassium-based internal recording solution containing (in mM): 130.0 K-gluconate, 4.0 KCl, 2.0 NaCl, 10 HEPES, 0.2 EGTA, 4.0 ATP-Mg, and 0.3 GTP-Tris, 14.0 phosphocreatine-K (pH 7.25, ~290 mOsm). During all recordings, pipette capacitances were neutralized. Series resistances (~12-32) were compensated online (100% for current-clamp, 60-70% for voltage-clamp). Pharmacological agents (stated in the figure legends when utilized) were diluted in ACSF just before use and applied though the bathing solution. Voltages reported here were corrected for a -14 mV liquid junction potential. The reversal potential for $GABA_A$ receptor-mediated responses in thalamic relay cells was -91 mV.

Measurements of Intrinsic Physiological Properties: Resting membrane potentials were measured within 2 min of break-in. Steady-state potentials were adjusted to -74 mV or -84 mV with intracellular current to test physiological properties in tonic or burst mode, respectively. Input Resistances (R_{in}) and membrane time constants (τ_m) were calculated from voltage responses (~3 mV deflections) to small negative current injections (3-25 pA, 600 ms). For τ_m, the voltage responses were fitted with a single exponential to the initial 50 ms of the response, omitting the

first ms. R_{in} values were measured using Ohms law and input capacitances C_{in} were calculated as τ_m / R_{in}.

Threshold (rheobase) currents were measured as the minimum injected currents required to discharge an AP (determined using 1 sec duration currents, 5 pA step increments). All other action potential (AP) and after-AP properties were measured from the first AP discharged at the threshold current, but APs were only analyzed if discharged in the initial 200 ms). AP voltage thresholds were measured, and verified by visual inspection, as the potential at which the rate of rise was greater than 10 V/s. AP amplitudes and after-AP properties were measured relative to the threshold potential. AP widths were measured at half of the AP amplitude (threshold voltage to peak). Fast afterhyperpolarizations (fast AHPs) were measured as the most hyperpolarized potential immediately succeeding the AP. In tonic mode, afterdepolarizations (ADPs) were measured as the most depolarized potential within 20 ms of the AP, and slow AHPs (sAHPs) were measured as the most hyperpolarized potential within 100 ms after the ADP. In burst mode, the AHP following the burst was measured as the minimum potential within 150 ms following the burst. ADP and sAHP measurements were not considered if a second AP (or tonic APs after a burst) confounded the measurements.

Repetitive spiking properties in tonic and burst mode were measured using positive current steps (25-200 pA, 25 pA increments, 1 s duration). Spike frequency adaptation was measured by calculating the adaptation ratio (frequency of the last 2 APs divided by the frequency of the first 2 APs) averaged across all sweeps in which the frequency of the last 2 APs was 20-60 Hz.

To elicit offset bursts (Fig. 3, Extended Data Fig. 16 and Extended Data Table 1), the steady-state potential was adjusted to -74 mV with intracellular current, then 1 s duration negative currents were injected. Offset bursts were measured from trials in which negative current (20-300 pA, 20-25 pA increments) led to an average voltage of -92 ± 2 mV at the end of the current step.

<u>Photostimulation</u>: The majority of synaptic physiology experiments focused on inputs to TRN cells from excitatory thalamic relay neurons, although inhibitory outputs of TRN cells to thalamic relay neurons were also characterized. In either case, ChR2 was optically excited using high power white light-emitting diodes (LEDs) (Mightex LCS-5500-03-22) controlled by Mightex LED controllers (SLCAA02-US or BLS-1000-2). The light was collimated and reflected through a 40X water immersion objective, resulting in a spot diameter of ~400 µm and a maximum LED power at the focal plane of 29.2 mW. The stimuli, delivered as 10 Hz trains of 1 ms flashes, were typically directed at ChR2-expressing presynaptic terminals by centering the light spot over the recorded postsynaptic cells (the postsynaptic cells did not express ChR2).

In a subset of experiments (Extended Data Fig. 12), within-cell comparisons were made of TRN cell responses to stimulation directed at opsin-expressing presynaptic axons/terminals (from VP or POM) versus stimulation directed further upstream at the VP or POM cell bodies of origin.

Simulated Synaptic Current Injections: Simulated synaptic current waveforms for thalamic (VP and POM) inputs to TRN were generated from averaged measurements of optogenetically evoked synaptic responses (recorded in voltage clamp at -84 mV) from Central and Edge TRN cells. These simulated synaptic currents for VP and POM inputs were matched for total synaptic charge across the 10 Hz trains (49.5 pC) and injected into the Central and Edge TRN cells to test features of integration in each cell type (described in the main text and legend of Fig. 4).

Data Analysis: Analysis of electrophysiogical data was performed in CED Signal 6, Molecular Devices Clampfit 10, Matlab, and Microsoft Excel. Analysis of anatomical data was performed in ImageJ (plugins used: CellCounter, ROIManager, bUnwarpJ), and Microsoft Excel.

Statistical Analysis: Statistical comparisons were performed in GraphPad Prism7 or SigmaPlot. Statistical tests used are indicated in the Results and Figure Legends. Data are represented as mean ± SEM, and statistical significance was defined as $p < 0.05$, unless otherwise noted in the results.

* Agmon, A. & Connors, B. W. Thalamocortical responses of mouse somatosensory (barrel) cortex in vitro. *Neuroscience* **41**, 365-379 (1991).